

# Studying Independent *Kcna6* Knock-out Mice Reveals Toxicity of Exogenous LacZ to Central Nociceptor Terminals and Differential Effects of Kv1.6 on Acute and Neuropathic Pain Sensation

Liam J. Peck,<sup>1</sup> Ryan Patel,<sup>2</sup> Paula Diaz,<sup>3</sup> Yolanda M. Wintle,<sup>1</sup> Anthony H. Dickenson,<sup>2</sup> Andrew J. Todd,<sup>4</sup> Margarita Calvo,<sup>3\*</sup> and David L.H. Bennett<sup>1\*</sup>

<sup>1</sup>Nuffield Department of Clinical Neurosciences, University of Oxford, Oxford, OX3 9DU, United Kingdom, <sup>2</sup>Department of Neuroscience, Physiology and Pharmacology, University College London, London, WC1E 6BT, United Kingdom, <sup>3</sup>Departamento de Fisiología, Facultad de Ciencias Biológicas, Pontificia Universidad Católica de Chile and Millennium Nucleus for the Study of Pain, Santiago, 8330025, Chile, and <sup>4</sup>Institute of Neuroscience and Psychology, University of Glasgow, Glasgow, G12 8QQ, United Kingdom

The potassium channel Kv1.6 has recently been implicated as a major modulatory channel subunit expressed in primary nociceptors. Furthermore, its expression at juxtaparanodes of myelinated primary afferents is induced following traumatic nerve injury as part of an endogenous mechanism to reduce hyperexcitability and pain-related hypersensitivity. In this study, we compared two mouse models of constitutive Kv1.6 knock-out (KO) achieved by different methods: traditional gene trap via homologous recombination and CRISPR-mediated excision. Both Kv1.6 KO mouse lines exhibited an unexpected reduction in sensitivity to noxious heat stimuli, to differing extents: the Kv1.6 mice produced via gene trap had a far more significant hyposensitivity. These mice (*Kcna6<sup>lacZ</sup>*) expressed the bacterial reporter enzyme LacZ in place of Kv1.6 as a result of the gene trap mechanism, and we found that their central primary afferent pre-synaptic terminals developed a striking neurodegenerative phenotype involving accumulation of lipid species, development of “meganeurites,” and impaired transmission to dorsal horn wide dynamic range neurons. The anatomic defects were absent in CRISPR-mediated Kv1.6 KO mice (*Kcna6<sup>-/-</sup>*) but were present in a third mouse model expressing exogenous LacZ in nociceptors under the control of a Nav1.8-promoted Cre recombinase. LacZ reporter enzymes are thus intrinsically neurotoxic to sensory neurons and may induce pathologic defects in transgenic mice, which has confounding implications for the interpretation of gene KOs using *lacZ*. Nonetheless, in *Kcna6<sup>-/-</sup>* mice not affected by LacZ, we demonstrated a significant role for Kv1.6 regulating acute noxious thermal sensitivity, and both mechanical and thermal pain-related hypersensitivity after nerve injury.

**Key words:** gangliosides; Kv1.6; LacZ; neuropathic pain; nociception; pain

## Significance Statement

In recent decades, the expansion of technologies to experimentally manipulate the rodent genome has contributed significantly to the field of neuroscience. While introduction of enzymatic or fluorescent reporter proteins to label neuronal populations is now commonplace, often potential toxicity effects are not fully considered. We show a role of Kv1.6 in acute and neuropathic pain states through analysis of two mouse models lacking Kv1.6 potassium channels: one with additional expression of LacZ and one without. We show that LacZ reporter enzymes induce unintended defects in sensory neurons, with an impact on behavioral data outcomes. To summarize we highlight the importance of Kv1.6 in recovery of normal sensory function following nerve injury, and careful interpretation of data from LacZ reporter models.

Received Jan. 25, 2021; revised Aug. 19, 2021; accepted Aug. 20, 2021.

Author contributions: L.J.P., A.H.D., A.J.T., M.C., and D.L.H.B. designed research; L.J.P., R.P., P.D., Y.M.W., A.J.T., and M.C. performed research; L.J.P., R.P., P.D., Y.M.W., A.J.T., and M.C. analyzed data; L.J.P. wrote the first draft of the paper; L.J.P., R.P., A.H.D., A.J.T., M.C., and D.L.H.B. edited the paper; L.J.P. and D.L.H.B. wrote the paper.

D.L.H.B. is a Wellcome senior clinical scientist (Grant 202747/Z/16/Z). L.J.P. was supported by a Wellcome OXION DPhil Studentship (Grant 109117/Z/15/Z). A.J.T. was supported by a Wellcome investigator award (Grant 219433/Z/19/Z). A.J.T., A.H.D., and R.P. were supported by the Wellcome Pain Consortium (Grant 102645/Z/13/Z). M.C. was supported by Millennium Nucleus for the Study of Pain, Millennium Science Initiative of the Ministry of Science, Technology, Knowledge and Innovation (Chile). This work was supported in whole, or in part, by Wellcome Trust Grants 109117/Z/15/Z, 202747/Z/16/Z, 219433/Z/19/Z, and 102645/Z/13/Z. For the purpose of open access, the author

has applied a CC BY public copyright license to any author accepted manuscript version arising from this submission. We thank Prof. John N. Wood (University College London) for provision of Nav1.8 Cre mice; and Dr. Juliet Gray (University of Southampton) for provision of mouse monoclonal anti-GD2 antibodies.

The authors declare no competing financial interests.

\*M.C. and D.L.H.B. contributed equally to this work.

Correspondence should be addressed to Liam J. Peck at liam.peck@sjc.ox.ac.uk or David L. H. Bennett at david.bennett@ndcn.ox.ac.uk.

<https://doi.org/10.1523/JNEUROSCI.0187-21.2021>

Copyright © 2021 the authors

## Introduction

The *Shaker*-like Kv1 potassium channel family comprises 8  $\alpha$  subunits (Kv1.1–Kv1.8), each considered a mammalian homolog of the *Shaker* channel that produced hyperexcitable sensorimotor phenotypes in *Drosophila* when mutated. These channels have also been shown to be key regulators of neuronal excitability in mammals (Browne et al., 1994; Smart et al., 1998; Robbins and Tempel, 2012). The most comprehensive recent reports indicate that Kv1.1, Kv1.2, Kv1.4, and Kv1.6 are expressed in mouse sensory neurons (Zeisel et al., 2018; Zheng et al., 2019). Although mouse KO studies have shown that Kv1.1 and Kv1.2 regulate dorsal root ganglion (DRG) neuron excitability, there have been few studies of the role of Kv1.6 (encoded by *Kcna6*) in DRG neurons and in sensory coding.

Recent single-cell transcriptomic approaches detected expression of *Kcna6* mRNA throughout the mouse nervous system (Usoskin et al., 2015; Häring et al., 2018; Zeisel et al., 2018) and, within sensory ganglia, *Kcna6* is reported to be the second most abundant potassium channel subunit in nociceptive populations (Zheng et al., 2019). Blockade of Kv1.1/1.2/1.6-containing channels by  $\alpha$ -dendrotoxin in Mrgprd-expressing neurons increased the repetitive firing capability of these nociceptive neurons *in vitro* (Zheng et al., 2019).

Kv1.6 is upregulated in rodent and human myelinated primary somatosensory neurons after peripheral nerve injury (Calvo et al., 2016). Under these conditions, Kv1.6 subunits emerge at neuronal sites flanking the node of Ranvier and replace native subunits Kv1.1 and Kv1.2, which are known to be downregulated transcriptionally and at the protein level shortly after peripheral nerve injury (Ishikawa et al., 1999; Zhao et al., 2013; Calvo et al., 2016; Hong et al., 2016; González et al., 2017). The timing of Kv1.6 appearance at the juxtaparanode (JXP) and paranode corresponds with both a reduction of ectopic electrical activity and improved withdrawal thresholds for reflexes evoked mechanically by von Frey hairs (Calvo et al., 2016). However, both of these recovery effects were reversed by pharmacological blockade of Kv1.6-containing channels with local application of  $\alpha$ -dendrotoxin (Calvo et al., 2016). It is therefore suggested that Kv1.6 subunits are involved in a compensatory response to peripheral nerve injury.

These data suggest that Kv1.6-containing channels provide “brake”-like counter currents that oppose neural excitation in sensory neurons, as described for other Kv1 subunits (Madrid et al., 2009; Hao et al., 2013; Zhao et al., 2013; González et al., 2017; Dawes et al., 2018). In this study, we have sought to detail the expression of *Kcna6* in the mouse sensory neuraxis, with a predominant focus on primary afferent neurons of the DRGs. In addition to this, through a global gene KO strategy, we have studied sensorimotor behavior in two *Kcna6*-null mouse strains (termed *Kcna6<sup>lacZ/lacZ</sup>* and *Kcna6<sup>-/-</sup>*) to identify a role for Kv1.6-containing channels in pain and/or somatosensation in the contexts of acute and neuropathic pain. Surprisingly, results were not consistent between *Kcna6* KO strains; and we provide anatomic, electrophysiological, and behavioral evidence that the presence or absence of exogenous *lacZ* reporter cassettes accounts for the phenotypic differences between these two mouse strains. Furthermore, we show that expression of *lacZ* alone on an otherwise phenotypically normal background is sufficient to cause deleterious effects to nociceptive presynaptic terminals in the dorsal horn. Notwithstanding these unexpected consequences of genetic manipulation, the findings of this study support a role for *Kcna6* in acute noxious thermal sensation and in contributing to recovery of normal sensory function in a neuropathic pain model.

## Materials and Methods

### Animals

Behavioral experiments involving the use of uninjured mice were performed in compliance with the Animals (Scientific Procedures) Act 1986, under UK Home Office-issued project licenses 30/3015 and P1DBEBAB9 held by Prof. David Bennett at the University of Oxford. Behavioral experiments involving the chronic constriction injury (CCI) model of neuropathy were performed at Pontificia Universidad Católica de Chile and approved by the Institutional Ethics Committee (protocol ID 150714013). *In vivo* electrophysiological experiments were performed at University College London under UK Home Office project license PEB669065 held by Prof. Anthony Dickenson. Male and female mice were used throughout.

*Kcna6<sup>lacZ</sup>* mice: *Kcna6<sup>tm1Lex</sup>/Mmucd* mice were purchased from MMRR (RRID:MMRR\_011729-UCD) on a mixed C57BL/6J;129S5 background, with heterozygote or WT littermates used as controls in all experiments. The *Kcna6<sup>tm1Lex</sup>* allele was produced by Lexicon Genetics (now Lexicon Pharmaceuticals) by homologous recombination of a gene trap cassette, containing *lacZ/neo* selection genes, with the coding sequence of *Kcna6* exon 1, depicted in Figure 3A. *Kcna6<sup>lacZ/lacZ</sup>*, *Advillin-EGFP* mice: In order to label primary afferent terminals within the spinal cord, the *Kcna6<sup>lacZ</sup>* strain was interbred with a mouse strain expressing a BAC transgene encoding EGFP under the *Advillin* promoter, Tg(Advillin-EGFP)QD84Gsat/Mmucd (RRID:MMRR\_034769-UCD). *Kcna6<sup>-/-</sup>* mice: *Kcna6<sup>tm1(MPC)</sup>/Mmjax* mice were purchased from MMRR (RRID:MMRR\_042391-JAX) and maintained on a C57BL/6N background, with heterozygote or WT littermates used as controls in all experiments. The nature of the mutation is Cas9-mediated excision of the sole coding region, leaving the initial 7 residues intact and resulting in frame shift and premature STOP codon. *Nav1.8<sup>Cre/+</sup>*; *ROSA26<sup>lacZ/+</sup>* mice: The *Gt(ROSA)26Sor<sup>tm1Sor</sup>/J* mouse is a conditional-ready strain carrying a *loxP-neo-poly A-loxP-lacZ* cassette in the ubiquitously expressed *ROSA26* locus (Soriano, 1999). Thus, there is ubiquitous expression of neomycin phosphotransferase (*neo*), followed by a *poly A* tail, which ordinarily prevents read-through transcription of *lacZ*. The *neo-poly A* sequence is flanked by *loxP* sites, so Cre-mediated recombination excises this region and results in expression only of *lacZ*. Homozygous conditional-ready *Gt(ROSA)26Sor<sup>tm1Sor</sup>/J* mice were gifted kindly by Prof. Shankar Srinivas (DPAG, University of Oxford) to serve as founders of the *Nav1.8<sup>Cre/+</sup>*; *ROSA26<sup>lacZ/+</sup>* colony by crossing with in-house heterozygous *Nav1.8<sup>Cre/+</sup>*; *ROSA26<sup>lacZ/+</sup>* mice (Nassar et al., 2004; Stirling et al., 2005) gifted by Prof. John Wood, University College London. This produced compound heterozygotes expressing one *lacZ* allele at the *ROSA26* locus in *Nav1.8*-positive neurons. *Nav1.8<sup>Cre</sup>*-negative littermates did not conditionally express *LacZ* but constitutively expressed a neomycin phosphotransferase cassette at the *ROSA26* locus.

### Tissue preparation for immunohistochemistry and *in situ* hybridisation (ISH)

To extract tissue for cryo-sectioning, animals were culled by overdose of pentobarbital delivered via intraperitoneal injection, followed by transcardial perfusion with 15 ml sterile 0.9% w/v saline, then 20 ml 4% PFA in 0.1 M PB. Dissected tissues were postfixed in 4% PFA for varied duration depending on tissue, as determined previously in our laboratory (Dawes et al., 2018): L4 DRG, 2 h (room temperature [RT]); spinal cord, 24 h (4°C); glabrous skin, 0.5 h (RT). For analysis of epidermal nerve fibers, skin was dissected from the glabrous region of the hind-paw proximal to the most proximal touch dome, as depicted in Figure 6A. After fixation, tissue was transferred to 30% sucrose in 0.1 M PB at 4°C for at least 24 h. Subsequently, tissue was embedded in OCT medium (TissueTek), rapidly frozen with liquid nitrogen, and stored at –80°C before cryo-sectioning. Sections were slide-mounted on Thermo Scientific SuperFrost Plus slides, with sections cut using a Leica cryostat (Leica Microsystems), at tissue-dependent thickness: DRG, 10  $\mu$ m; spinal cord, 20  $\mu$ m; skin, 14  $\mu$ m.

### ISH

Expression of *Kcna6* mRNA was investigated using a chromogenic ISH assay (RNAScope 2.5-RED, Advanced Cell Diagnostics). In brief, slides were removed from –80°C storage and allowed to equilibrate to room temperature before removal of OCT by submersion in DNAase/

RNAase-free PBS. Slides were pretreated with a 10 min application of H<sub>2</sub>O<sub>2</sub> at room temperature, washed with double-deionized Milli-Q water, submerged in 100% EtOH, and allowed to dry (20 min) before a 10 min application of protease plus in a humidified chamber at 40°C, followed by a further Milli-Q wash. The *Kcna6*-specific target detection probe (catalog #462821) was warmed in a 40°C water bath before a 2 h incubation on slides at 40°C, and the amplification steps and fast red reaction were performed according to the manufacturer's instructions. Following development of the red signal, slides were counterstained using the protocol described below.

#### Immunohistochemistry

Before antibody application, slides were washed and sections concurrently permeabilized in PBS + 0.3% Triton X-100. Primary antibodies were diluted in PBS containing 0.3% Triton X-100 and 5% goat or donkey blocking serum and incubated on sections overnight in a humidified chamber. The next day, unbound primary antibodies were washed off with PBS, and secondary antibodies were applied to sections for 2–3 h, followed by further washing in PBS and, in some instances where a biotinylated secondary antibody was used, a tertiary antibody incubation for up to 2 h. Finally, slides were mounted with glass coverslips and Vectashield mounting medium for fluorescence, and air-sealed with nail polish. For ganglioside antibody staining, slides were washed for 3 min in PBS + 0.1% Tween to avoid excess permeabilization; other steps in this protocol were the same as previously described for immunohistochemistry. Exact antibodies and dilutions used are detailed in Table 1.

#### Image acquisition

Fluorescence imaging was performed with a Carl Zeiss LSM700 confocal microscope. For quantification, images were generally acquired using a 20×, 40×, or 63× objective. Maximum intensity projections were produced from *z* stacks encompassing the entire section depth. For ISH experiments, image acquisition settings were kept the same for all quantified images to make signal comparable across sections.

#### RNA extraction and cDNA synthesis

Mice were culled by rising CO<sub>2</sub> concentration in a sealed chamber. Brains were rapidly dissected, immediately frozen in liquid nitrogen, and stored at –80°C. Tissue was homogenized in TriPure (Roche) and then treated with chloroform before column purification using a High Pure RNA isolation kit (Roche). RNA was eluted in RNAase-free water. Synthesis of cDNA was achieved using Transcriptor reverse transcriptase (Roche) with random hexamers (Invitrogen) and dNTPs (Roche).

#### qRT-PCR

Quantitative analysis of mRNA expression was conducted on a LightCycler 480 II system (Roche), using SYBR Green fluorescence for detection. Primers were designed using Primer-BLAST (<https://www.ncbi.nlm.nih.gov/tools/primer-blast/>) and were assessed for specificity and efficiency by melting curve analysis, and by serial dilution. Primers (0.5 μM) and cDNA (5 ng) were mixed with LightCycler 480 SYBR Green master mix (Roche) in a 1:1 ratio in 384-well plates and run on a 45-cycle protocol. All experimental samples were run in triplicate. Quantitation of expression was performed using the  $\delta\delta$  CT method (Livak and Schmittgen, 2001), and Kv1 gene products were first normalized to “housekeeping” genes (*Gapdh* and *Hprt1*) and then normalized to average WT expression per gene. Primer sequences are detailed in the Table 1.

#### Behavioral assays

Mice were housed in individually ventilated cages with no more than 6 or no fewer than 2 mice per cage, and fed *ad libitum*. The light-dark cycle period was 12 h, and behavioral experiments were performed during the light cycle. Multiple different behavioral assays were performed each day, but the time of day for each behavioral assay was kept constant. Before all experiments, animals were habituated to equipment so that the experimental environment was not novel during data collection. Unless otherwise stated, baseline results were averaged from three baseline recordings. Data from left and right hindlimb paws were combined and averaged for Hargreaves, von Frey, pin-prick, and dry ice results.

The experimenter was blinded to genotype at all times during behavioral testing and analysis. Details of individual assays are as follows:

**Open field.** Mice were placed in the corner of a 50 × 30 cm wooden box with a 5 × 3 grid marked on the base and allowed to move freely for 3 min. During this time, the number of grid lines crossed and hindlimb rearing episodes were recorded.

**Rotarod.** Mice were required to climb/walk against the direction of the platform (Ugo Basile) rotating at 28 rpm beneath them. The designated end point of this experiment was when the animal falls off the equipment, or at the 90 s mark, or when they cling to and rotate with the platform for 2 full revolutions cumulatively throughout the 90 s period.

**Beam test.** Mice were filmed from behind walking between two points along a thin cylindrical beam (~1.5 cm in diameter). The video footage was used to calculate the percentage of “incorrect” hindlimb steps (i.e., where hind-paws either slip or hop on the beam) from the total number of steps.

**Hot plate.** Animals were placed on the hot plate (Ugo Basile) set to either 50°C or 53°C, at which point a timer was started by depression of a foot switch. The time was recorded, and the animal removed, when the animal displayed visible pain behavior (hind-paw licking, biting, shaking, or jumping) or after a maximum of 20 s at maximal temperature of 53°C to avoid tissue injury.

**von Frey.** Mice were housed individually in Plexiglas enclosures on a metallic grille platform. After an acclimation period of between 30 min and 1 h, 50% mechanical withdrawal thresholds were derived using the Dixon up-and-down method (Dixon, 1965). Baseline measurements were averaged from left and right paw.

**Hargreaves.** Mice were housed individually in Plexiglas enclosures on a glass platform. An infrared heat source (Ugo Basile) was placed under the animal, targeted through the glass at the hind-paw. Switching on the heat source begins a timer, which turns off once the animal responds to the stimulus by relocating its paw. Otherwise, the test was stopped at a maximum of 20 s.

**Pin-prick.** Animals were temporally housed individually in Plexiglas chambers on a grille used for von Frey testing. A sharp pin was fixed to the filament of a 2.0 g von Frey hair and used to provide noxious punctate stimulation to left and right hind-paws. Withdrawal reflexes were filmed from below using an iPhone8 in slo-mo mode (720 p, 240 fps) such that still frames are ~4 ms apart. The withdrawal latency was derived *post hoc* by scrolling through frames from the time of contact with the paw to withdrawal. Two or occasionally three stimuli were applied to each paw on three separate baseline testing days, from which a mean baseline latency was calculated.

**Dry ice (cold plantar assay).** This assay has been described in detail previously (Brenner et al., 2012). Briefly, mice were housed individually in Plexiglas chambers on a 5 mm borosilicate glass surface (UQG Optics). Crushed dry ice pellets were compacted into a syringe with the tapered end cut off, such that the dry ice could be applied to the glass evenly beneath the hind-paw. A stopwatch was used to time the withdrawal latency.

#### Neuropathic model: CCI

CCI was performed as described previously (Bennett and Xie, 1988). Mice were anesthetized using isoflurane inhalation. The left sciatic nerve was exposed at the high-thigh level. Proximal to its trifurcation, three ligatures with 6-0 silk suture were tied loosely around the nerve at intervals of ~2 mm. The wound was closed with three external stitches and disinfected. All behavioral measurements were taken in awake and unrestrained mice of both sexes (2–4 months old). Two sessions of habituation (40–50 min each) to the testing area were conducted in 2 consecutive days followed by two baseline measurements of hind-paw withdrawal threshold in another 2 consecutive days. Groups were matched by sex and age. Mechanical and thermal sensitivity was assessed using von Frey hairs and the Hargreaves apparatus as previously described in this article. Thermal place preference (TPP) was additionally used as a parameter to assess thermal hypersensitivity. Mice were placed at the center of an apparatus that uses temperature adjustable plates. The reference plate was adjusted to set a neutral temperature at 25°C, whereas the other plate was adjusted to the specific noxious

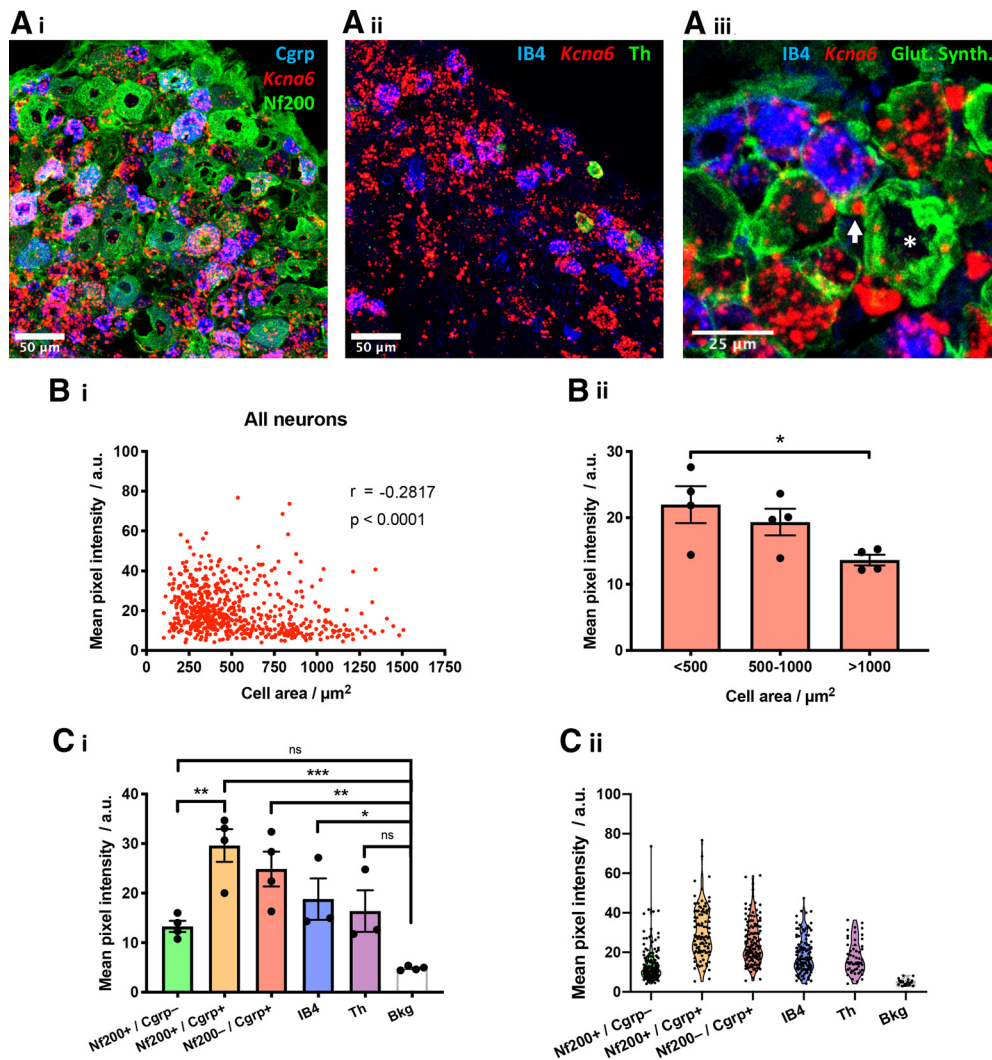


**Figure 1.** *Kcna6* mRNA is expressed in DRG neurons and satellite glia. **A**, Combined fluorescent ISH and immunohistochemistry reveal *Kcna6* mRNA expression in the lumbar (L4) DRGs. *Kcna6* in situ signal intensity was analyzed in L4 DRGs immunostained for neuronal markers: Nf200 and Cgrp (**Ai**), IB4 and Th (**Aii**), IB4 and satellite glial marker glutamine synthetase (**Aiii**). *Kcna6* is expressed in the Cgrp<sup>+</sup> and IB4-binding neuronal subpopulations and at a lower level in the Th population. Some expression in satellite glia ensheathing an IB4-labeled neuron (arrow) and a larger, IB4-negative neuron (asterisk) is indicated. Scale bars: **Ai, Aii, Aiii**, 50  $\mu\text{m}$ ; **Aiii**, 25  $\mu\text{m}$ . **Bi**, *Kcna6* expression across all DRG neurons analyzed from 4 animals is negatively correlated with cell size (nonparametric two-tailed Spearman's correlation,  $r = -0.2817$ ,  $p < 0.0001$ ). **Bii**, Small-diameter (<500  $\mu\text{m}^2$ ) DRG neurons had higher expression of *Kcna6* mRNA compared with large-diameter (>1000  $\mu\text{m}^2$ ) DRG neurons ( $n = 4$  WT animals per category). \* $p < 0.05$  (<500 vs >1000 [small vs large], ordinary one-way ANOVA with Tukey's *post hoc* multiple comparisons test). **Ci**, Differentiating DRG populations by histochemical markers reveals generally very low *Kcna6* expression in myelinated (Nf200<sup>+</sup>) neurons, but highest expression in myelinated peptidergic (Nf200<sup>+</sup>/Cgrp<sup>+</sup>) neurons. On per-animal analysis, expression is significantly above background (Bkg) in all nociceptive populations. Data points are mean values from individual replicates, plotted with overall WT mean  $\pm$  SEM;  $n = 4$  or 3 WT animals per category. \* $p < 0.05$ , \*\* $p < 0.01$ , \*\*\* $p < 0.001$ , one-way ANOVA with Tukey's *post hoc* multiple comparisons test. Bkg, Background signal from attached nerve root. **Cii**, Data points represent individual neurons, combined from all DRG sections from all animals.

temperature of interest (50°C or 53°C). The mouse was then allowed to move freely from plate to plate for 2 min. Movements were recorded by a camera mounted directly above the enclosed space. Data are expressed as the percentage of the time spent on the test plate.

#### Intraepidermal nerve fiber density

Following immunostaining, three sections each from 4 animals per *Kcna6*<sup>LacZ</sup> genotype were analyzed on a Carl Zeiss LSM700 confocal microscope. Using DAPI to mark the dermis/epidermis boundary, the number of Pgp9.5-immunoreactive fibers that could be visualized crossing from dermis to epidermis was counted through the viewfinder with a 63 $\times$  oil immersion lens. A *post hoc* overview image was taken, and the length of epidermis analyzed was measured in ZEN Black software; across all sections, this ranged between 2.1 and 3.3 mm.

#### DRG subpopulation counts and Atf3 expression

For subpopulation analysis, at least 2 whole DRG sections were imaged and analyzed per animal. DRG "profiles" were defined as being

Neurotrace-positive and nucleated. Profiles were designated positive or negative for histochemical markers by eye on images of whole DRG sections taken with identical acquisition settings, and their abundance was calculated as a percentage of Neurotrace-positive profiles (fluorescent Nissl stain). For Atf3 analysis, at least four randomly chosen fields of view were analyzed from DRGs dissected from 4 *Kcna6*<sup>LacZ/LacZ</sup> animals and 4 WT littermates.

#### Transmission electron microscopy (TEM)

Adult mice received an intraperitoneal overdose of pentobarbital and were then transcardially perfused with 0.9% saline followed by a 1% PFA, 1% glutaraldehyde fixative in 0.1 M PB. Spinal cords were then removed and postfixed in the same solution for 24 h and transferred to 0.1 M PB before sectioning; 60  $\mu\text{m}$  sections were prepared using a vibrating-blade microtome, postfixed with osmium tetroxide OsO<sub>4</sub>, dehydrated, and flat-embedded in epoxy resin. At this stage, some images were acquired using light microscopy. Subsequently, ultrathin sections were cut using a Diatome diamond knife and Leica Ultracut S

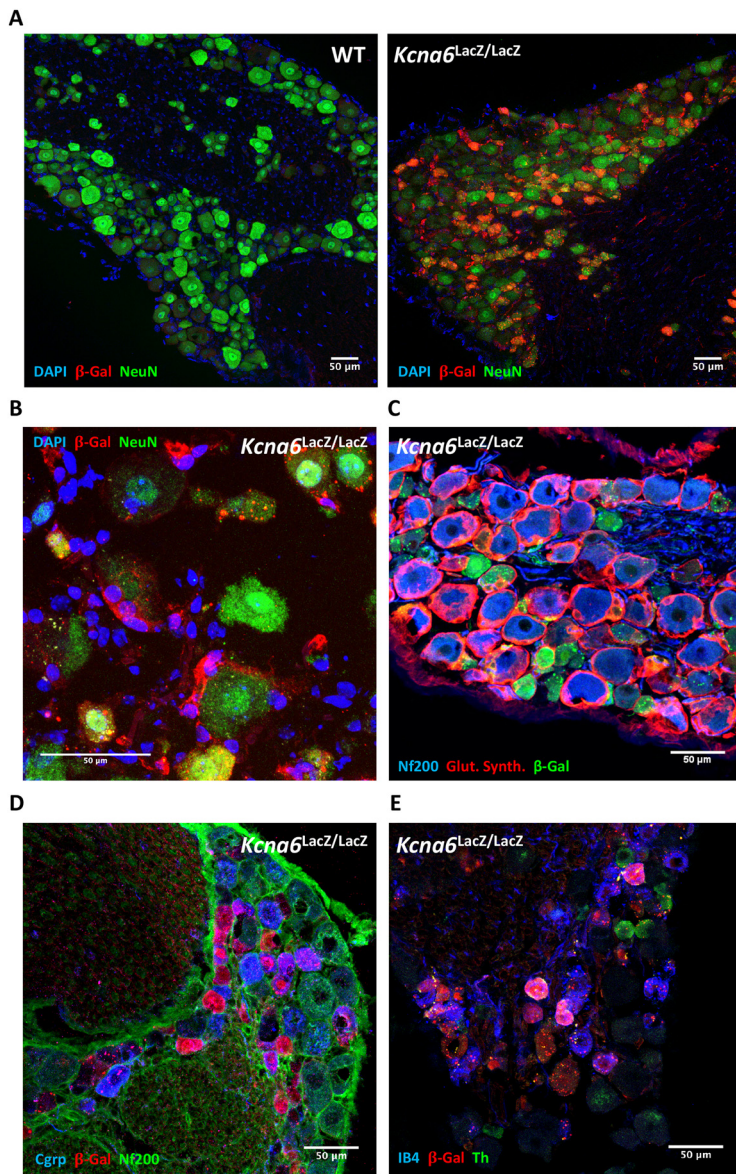


**Figure 2.** LacZ ( $\beta$ -galactosidase) expression in  $Kcna6^{lacZ/lacZ}$  DRG. **A**,  $Kcna6^{lacZ}$  carriers, but not WT littermates, express  $\beta$ -galactosidase under the  $Kcna6$  promoter, detectable in DRG cells by immunostaining. **B**, In addition to prominent  $\beta$ -galactosidase immunoreactivity in small neurons, staining revealed LacZ-expressing satellite glia ensheathing DRG neurons, confirmed with an antibody raised against satellite glial marker, glutamine synthetase (**C**). **D**, **E**, The  $Cgrp^+$  ( $\pm Nf200^+$ ),  $IB4^+$ , and  $Th^+$  populations were all positive for  $\beta$ -galactosidase. Scale bars, 50  $\mu$ m.

ultramicrotome. Images were acquired at 120 kV on a Philips CM100 transmission electron microscope with a Gatan OneView CMOS camera. The appearance of identifiable glomerular structures was interpreted qualitatively.

#### *In vivo dorsal horn recordings*

Both male and female  $Kcna6^{+/+}$ ,  $Kcna6^{lacZ/+}$ , and  $Kcna6^{lacZ/lacZ}$  littermate mice were used; the mean  $\pm$  SD ages of animals were as follows:  $17.3 \pm 3.3$  ( $Kcna6^{+/+}$ ),  $14.7 \pm 1.1$  ( $Kcna6^{lacZ/+}$ ), and  $17.1 \pm 2.5$  ( $Kcna6^{lacZ/lacZ}$ ) weeks. Mice were initially anesthetized with 3.5% v/v isoflurane delivered in 3:2 ratio of nitrous oxide and oxygen. Once areflexic, mice were secured in a stereotaxic frame and subsequently maintained on 1.5% v/v isoflurane for the remainder of the experiment ( $\sim$ 4 h in duration). Core body temperature was maintained with the use of a homeothermic blanket, and respiratory rate was visually monitored throughout. A laminectomy was performed to expose the L3–L5 segments of the spinal cord; mineral oil was then applied to prevent

dehydration. Extracellular recordings were made from deep dorsal horn wide dynamic range (WDR) neurons with receptive fields on the glabrous skin of the toes using 0.127 mm 2 M $\Omega$  Parylene-coated tungsten electrodes (A-M Systems). Searching involved light tapping of the hind-paw while manually moving the electrode. All recordings were made at depths delineating the deep dorsal horn laminae (Watson et al., 2009), and were classified as WDR on the basis of neuronal sensitivity to dynamic brushing (i.e., gentle stroking with a squirrel-hair brush), and noxious punctate mechanical (15 g) and heat (48°C) stimulation of the receptive field.

The receptive field was then stimulated using a wider range of natural stimuli (brush, von Frey filaments 0.4, 1, 4, 8, and 15 g, and heat 32°C, 42°C, 45°C, and 48°C) applied over a period of 10 s per stimulus and the evoked response quantified. The heat stimulus was applied with a constant water jet onto the center of the receptive field. Ethyl chloride (50  $\mu$ l) was applied to the receptive field, described previously as an evaporative noxious cooling stimulus (Leith et al., 2010). Evoked responses to room temperature water (25°C) were subtracted from ethyl chloride-evoked responses to control for any concomitant mechanical stimulation during application. Natural stimuli were applied starting with the lowest intensity stimulus with  $\sim$ 40 s between stimuli in the following order: brush, von Frey, cold, heat, electrical. Receptive fields were determined using a 15 g von Frey. An area was considered part of the receptive field if a response of  $>30$  action potentials over 5 s was obtained. A rest period of 30 s between applications was used to avoid sensitization. Receptive field sizes are expressed as a percentage area of a standardized paw measured using ImageJ (National Institutes of Health). Electrical stimulation of WDR neurons was delivered transcutaneously via needles inserted into the receptive field. A train of 16 electrical stimuli (2 ms pulses, 0.5 Hz) was applied at 3 times the threshold current for C-fiber activation. Responses evoked by A- (0–50 ms) and C-fibers (50–250 ms) were separated and quantified on the basis of latency. Neuronal responses occurring after the C-fiber latency band were classed as postdischarge. The input and the wind-up were calculated as follows: [Input = action potentials evoked by first pulse  $\times$  total number of pulses] and [Wind up = total action potentials after 16 train stimulus – Input].

The signal was amplified ( $\times 6000$ ), bandpass filtered (low-/high-frequency cutoff 0.5/2 kHz), and digitized at rate of 20 kHz. Data were captured and analyzed by a Cambridge Electronic Design 1401 interface coupled to a computer with Spike2 software with poststimulus time histogram and rate functions. In some cases where a single-unit recording could not be obtained, spike sorting was performed *post hoc* with Spike2 using fast Fourier transform followed by three-dimensional principal component analysis of waveform features for multiunit discrimination (electrical stimulation was not performed for these neurons). One to three neurons were characterized per mouse. In total, 19 neurons were characterized from 14 WT mice (7 male, 7 female), 21 neurons from 16  $Kcna6^{lacZ/+}$  mice (10 male, 6 female), and 19 neurons from 15  $Kcna6^{lacZ/lacZ}$  mice (6 male, 9 female). Of these neurons, 15 per genotype were successfully stimulated transcutaneously so that electrical properties could be interrogated. *In vivo* electrophysiological procedures were nonrecovery; at the end of experiments, mice were terminally anesthetized with isoflurane.

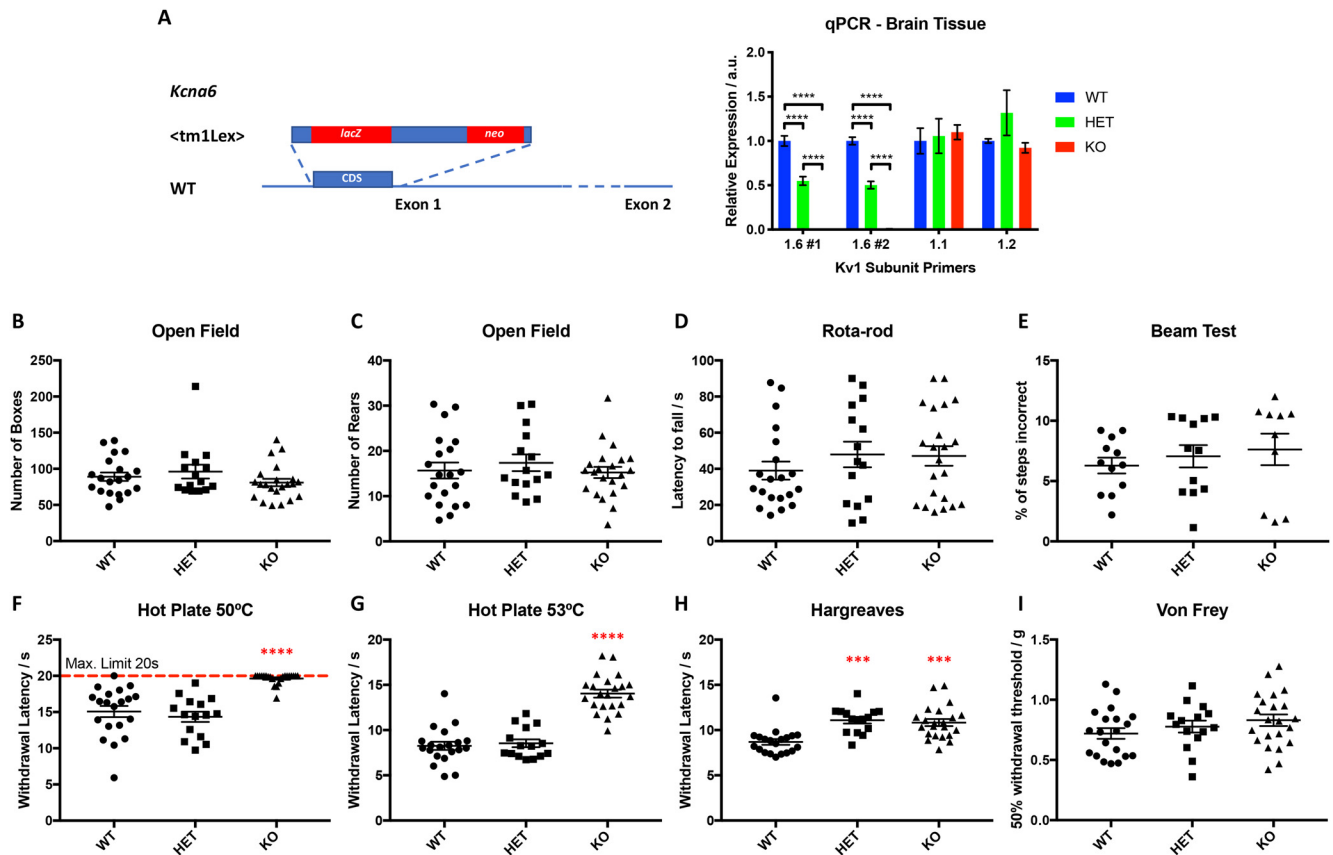


**Figure 3.** *Kcna6<sup>lacZ</sup>* mice are hyporesponsive to noxious heat. **A**, The <tm1Lex> vector, containing a *lacZ* cassette, is introduced to the coding sequence (CDS) of *Kcna6* exon 1 by homologous recombination, resulting in *Kcna6* KO as confirmed by qRT-PCR (a.u., arbitrary units relative to WT expression) on brain RNA extract using 2 sets of primers. Expression of two other Kv1 subunits (Kv1.1 and Kv1.2) is unaffected by *Kcna6* KO.  $n = 4$  WT, 3 HET, 4 KO. \*\*\*\* $p < 0.0001$  (ordinary one-way ANOVA with Tukey's *post hoc* multiple comparisons test). **B–E**, *Kcna6<sup>lacZ/+</sup>* and *lacZ/lacZ* mice perform normally on open field and motor function tests. **F–H**, *Kcna6<sup>lacZ/lacZ</sup>* mice are hyporesponsive on 50°C and 53°C hot plate assays, while both heterozygous and homozygous mutants are hyporesponsive on the Hargreaves radiant heat assay. **I**, Neither groups differ from WT in their response to mechanical stimulation by von Frey hairs. Data points represent individual animal values, plotted with group mean  $\pm$  SEM.  $n = 20$  *Kcna6<sup>+/+</sup>* (11 male, 11 female), 15 *Kcna6<sup>lacZ/+</sup>* (13 male, 2 female), 22 *Kcna6<sup>lacZ/lacZ</sup>* (11 male, 11 female), apart from the beam test (**E**);  $n = 12$  *Kcna6<sup>+/+</sup>* (6 male, 6 female), 12 *Kcna6<sup>lacZ/+</sup>* (10 male, 2 female), 10 *Kcna6<sup>lacZ/lacZ</sup>* (6 male, 4 female). \*\*\* $p < 0.001$ , \*\*\*\* $p < 0.0001$  versus *Kcna6<sup>+/+</sup>* and *Kcna6<sup>lacZ/+</sup>* (**F,G**) or versus *Kcna6<sup>+/+</sup>* (**H**) (one-way ANOVA with Tukey's *post hoc* multiple comparisons test).

#### Experimental design and statistical analyses

GraphPad Prism software was used for all statistical calculations. In general, unless otherwise stated, the unit of statistical analysis was the individual animal and significance is reported as multiplicity-adjusted  $p$  values.  $N$  values and details of mouse sex are included in figure legends as appropriate.

**ISH.** Expression of *Kcna6* mRNA was quantified by calculating the mean red channel pixel intensity (converted from 0 to 255 8-bit color value to a percentage scale) in ROIs drawn in ImageJ software around cells with identifiable nuclei; thus, expression is normalized to cell size (sum of pixel intensities/number of pixels). “Background” was from ROIs containing nerve root. Mean *Kcna6* expression per animal was assessed for normality using the Shapiro–Wilk test and compared between categories by ordinary one-way ANOVA with Tukey's *post hoc* multiple comparisons test (see Fig. 1*Bii,Ci*).

**qRT-PCR.** Comparison of Kv1 subunit mRNA expression between *Kcna6<sup>lacZ</sup>* genotypes was performed using ordinary one-way ANOVA independently for each gene or primer, with Tukey's *post hoc* multiple comparisons test.

**Behavior.** Data are presented as group mean (grouped by genotype and/or time point)  $\pm$  SEM unless otherwise stated and include data points from individual animals. Data were first assessed for normality using the Shapiro–Wilk test. Baseline sensorimotor performance was compared between genotypes by one-way ANOVA. We used Dunnett's *post hoc* multiple comparisons test to identify differences relative to WT controls, or Tukey's *post hoc* test when reporting differences with all possible comparisons between genotypes. For CCI studies, a two-way repeated-measures ANOVA was used with Sidak multiple comparisons

test to compare genotypes at different time points. The unit of statistical analysis was the animal, and significance was reported as multiplicity-adjusted  $p$  values.

**Intra-epidermal nerve fiber density.** Samples were assessed for normality by Shapiro–Wilk test and means compared with a two-tailed, unpaired Student's  $t$  test.

**DRG populations.** Samples were assessed for normality by Shapiro–Wilk test, within each subpopulation. Multiple  $t$  tests were performed to compare WT and *Kcna6<sup>lacZ/lacZ</sup>* values for each subpopulation, corrected for with a false discovery rate of 5% using the recommended Benjamini, Krieger, and Yekutieli method in GraphPad Prism.

**In vivo electrophysiology.** In all experiments, the neuron was considered to be the experimental unit of replication. Minimum group sizes were determined by *a priori* calculations using the following assumptions ( $\alpha$  0.05,  $1-\beta$  0.8,  $\epsilon$  1, effect size range  $d = 0.5-0.8$ ). Effect sizes were based on historical datasets. Mechanical and heat responses were analyzed by two-way repeated-measures ANOVA with Dunnett's *post hoc* test to compare to WT results. Brush, cold, fiber threshold, electrical results, and receptive field were assessed for normality using the Shapiro–Wilk test. If they passed, each characteristic was assessed by one-way ANOVA with Dunnett's or Tukey's *post hoc* test to make multiple comparisons versus WT or between all genotypes, respectively. For characteristics that failed the normality test, a Kruskal–Wallis test was performed instead with Dunn's *post hoc* multiple comparisons test. Multiplicity-adjusted  $p$  values are reported in each case. Kinetics of windup was assessed by nonlinear regression, fitting a one-phase association curve to each data set and comparing the rate constant and plateau between each genotype.

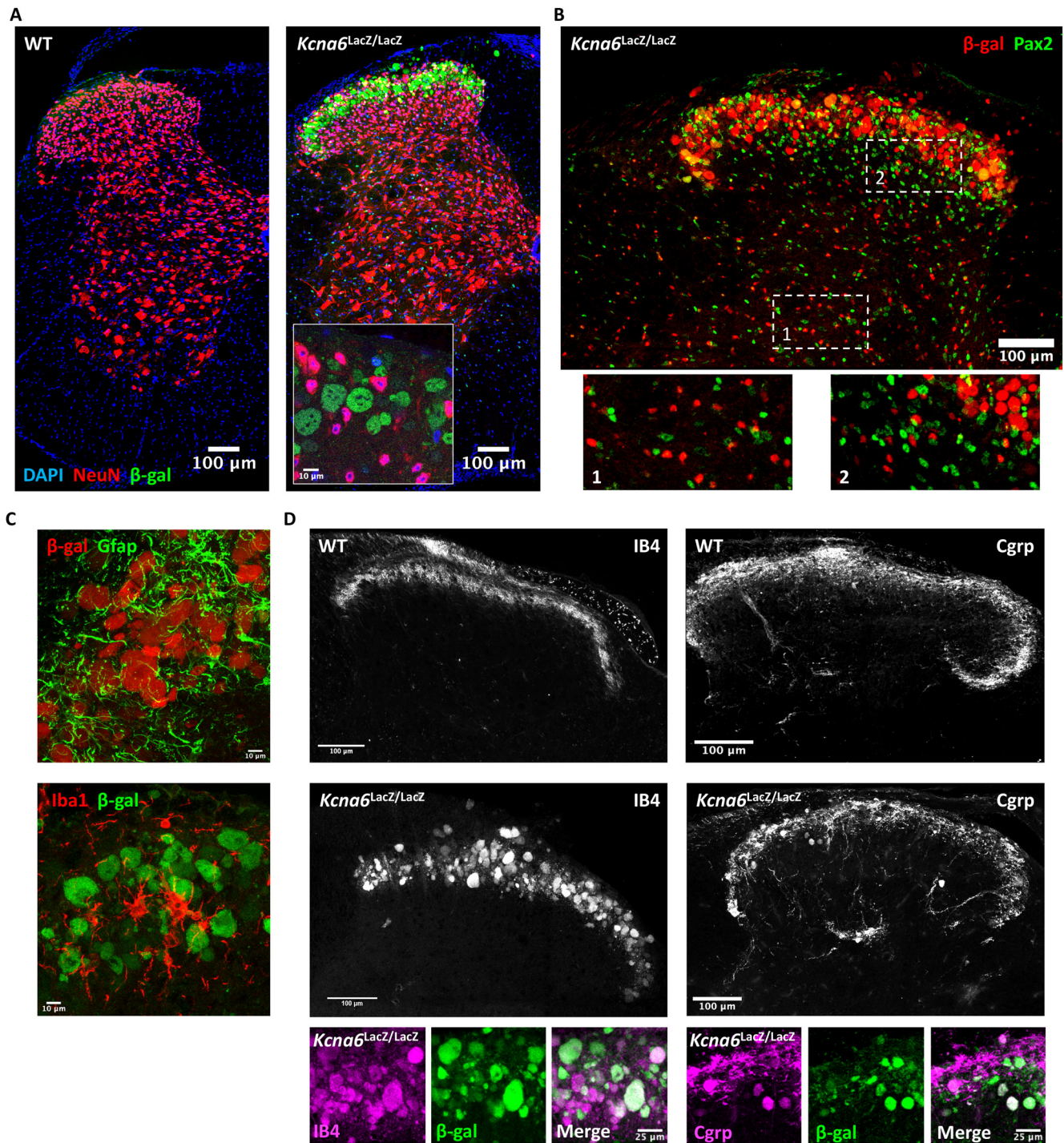


**Figure 4.** Abnormal anatomy in the *Kcna6<sup>lacZ</sup>* dorsal horn. **A**, LacZ ( $\beta$ -gal) staining in *Kcna6<sup>lacZ</sup>* homozygote spinal cord sections revealed striking abnormal, large profiles within superficial dorsal laminae. LacZ immunoreactivity also colocalized with smaller NeuN-negative, DAPI-positive profiles throughout gray and white matter. Inset, High-power (63 $\times$  objective) single z-slice image of abnormal swollen, vacuolated LacZ<sup>+</sup> profiles in laminae I-II. Scale bars: 100  $\mu$ m; inset, 10  $\mu$ m. **B**, Abnormal LacZ<sup>+</sup> profiles do not colocalize with Pax2 (a marker of inhibitory interneurons), nor do smaller LacZ<sup>+</sup> profiles in deeper gray and white matter. **C**, In superficial laminae, LacZ does not colocalize with markers of astrocytes (GFAP) or microglia (IBA1), but glial activation is often observed in close apposition to the abnormal LacZ<sup>+</sup> profiles. Scale bar, 10  $\mu$ m. **D**, Markers of nonpeptidergic (IB4) and peptidergic (Cgrp) nociceptive populations known to terminate in superficial laminae show strong colocalization with enlarged profiles in *Kcna6<sup>lacZ</sup>* homozygote spinal cord sections. Scale bars: 100  $\mu$ m; inset, 25  $\mu$ m.

## Results

### Expression of *Kcna6* in the mouse DRG

Using a chromogenic ISH protocol (ACD), we visualized *Kcna6* expression in WT mouse L4 DRG neurons (Fig. 1A). Overall *Kcna6* expression was higher in smaller versus larger DRG neuronal populations. Across all cells examined from 4 animals, there is a significant negative correlation between mean *Kcna6*

pixel intensity and cell area (Fig. 1Bi); and across biological replicates, small-diameter neurons had significantly greater expression than large-diameter neurons (Fig. 1Bii). We quantified *Kcna6* expression in five immunohistochemically defined subpopulations of sensory neurons: namely, myelinated neurons expressing neurofilament 200 (Nf200); peptidergic nociceptors expressing calcitonin gene-related peptide (Cgrp); C-low

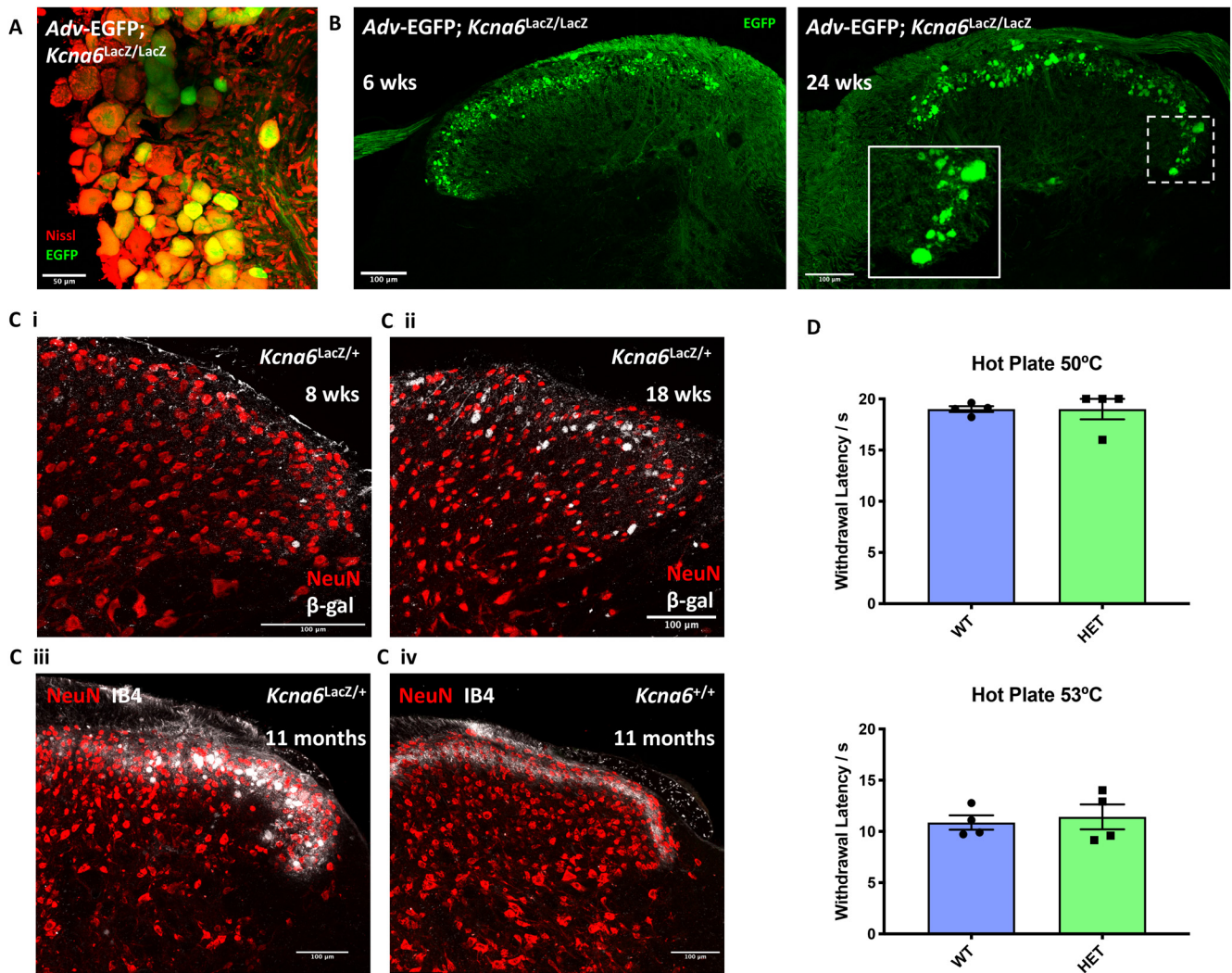


**Figure 5.** Degeneration of *Kcna6<sup>lacZ</sup>* primary afferents is progressive and gene dose-dependent. **A**, An *Advillin*-driven EGFP reporter mouse was crossed to the *Kcna6<sup>lacZ/lacZ</sup>* homozygotes to label DRG primary afferents marked by Nissl staining. Scale bar, 50  $\mu$ m. **B**, EGFP colocalized with the abnormal spinal profiles, confirming that they are primary afferent in origin. The pathology was present by 6 weeks postnatally but also appeared to worsen with age. Scale bar, 100  $\mu$ m. **C**, *Kcna6<sup>lacZ/+</sup>* heterozygotes had a late-onset, slowly progressing pathology over a period of 11 months, evidenced by LacZ (**Ci,Cii**) or IB4 (**Ciii**) staining, whereas WT were unaffected at 11 months (**Civ**). Scale bar, 100  $\mu$ m. **D**, At 11 months, despite developing primary afferent terminal pathology, *Kcna6<sup>lacZ/+</sup>* heterozygote mice did not display any behavioral hyposensitivity to noxious heat compared with WT age-matched littermate controls.  $n = 4$  *Kcna6<sup>+/+</sup>*, 4 *Kcna6<sup>lacZ/+</sup>* (2 male, 2 female per genotype).  $p = 0.8451$  (50°C) and  $p = 0.7273$  (53°C) by unpaired, two-tailed *t* test.

threshold mechanoreceptors expressing tyrosine hydroxylase ( $\text{Th}^+$  C-LTMRs); and nonpeptidergic nociceptors binding to isolectin B4 (IB4). Overlap between the  $\text{Nf200}^+$  and  $\text{Cgrp}^+$  population demarcates the fifth subpopulation of myelinated peptidergic nociceptors. Signal from the ISH was detected significantly above background fluorescence in nociceptive populations but not in the  $\text{Th}^+$  or  $\text{Nf200}^+/\text{Cgrp}^-$  populations (Fig. 1C). The strongest expression of *Kcna6* was observed in myelinated peptidergic neurons ( $\text{Nf200}^+/\text{Cgrp}^+$ ). We also noted *Kcna6* expression in satellite glial cells ensheathing DRG neurons, as identified by staining for glutamine synthetase (Figs. 1A and 2).

#### *Kcna6<sup>lacZ</sup>* KO mice exhibit altered nociceptive behavior

In order to investigate the contribution of Kv1.6 subunits to pain-like behavior in mice, we procured a *Kcna6* KO mouse produced by homologous recombination with a  $\langle \text{tm1Lex} \rangle$  cassette containing a *lacZ* reporter allele and neomycin phosphotransferase, henceforth termed *Kcna6<sup>lacZ</sup>* (MMRRC stock #011729-UCD). We confirmed expression of LacZ

protein ( $\beta$ -galactosidase) by immunohistochemical detection in appropriate DRG populations and satellite glia (Fig. 2), and complete loss of *Kcna6* mRNA in brain tissue by qRT-PCR (Fig. 3A).

Behavioral phenotyping of this KO strain included an array of sensorimotor assays. Heterozygous or homozygous *Kcna6<sup>lacZ</sup>* mice performed comparably to WT littermates on open field assays and motor coordination tasks (Fig. 3B–E). Homozygous *Kcna6<sup>lacZ/lacZ</sup>* KO mice had a striking deficit in noxious thermal sensitivity on both hot plate (50°C and 53°C) and Hargreaves assays, whereas heterozygous littermates were hyposensitive only to stimulation via the Hargreaves test (Fig. 3F–H). Responsiveness to light punctate mechanical stimuli via von Frey hair application was unaltered in either genotype compared with WT littermates (Fig. 3I).

#### *Kcna6<sup>lacZ</sup>* mice develop abnormal synapse-forming primary afferent terminals in the superficial dorsal horn

The most striking finding was a gross anatomic abnormality in the spinal dorsal horn of *Kcna6<sup>lacZ</sup>* mice. These abnormalities



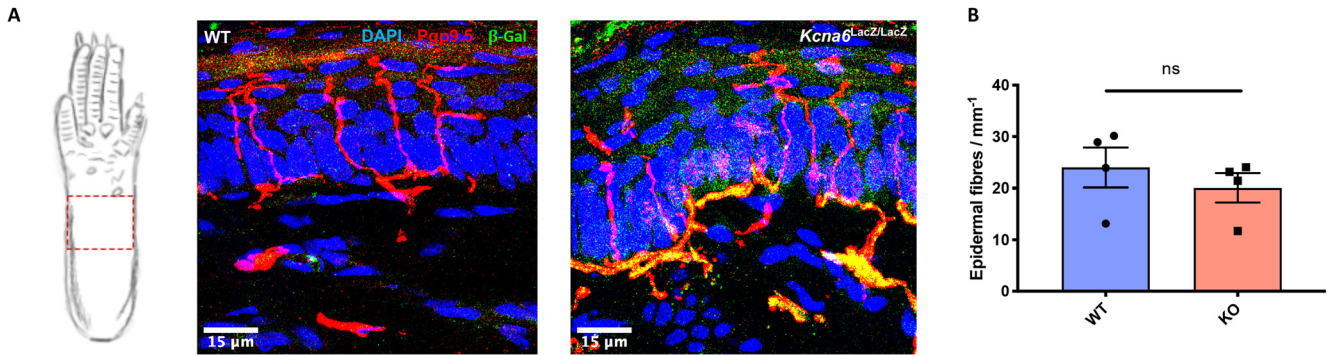


**Figure 6.** Intraepidermal nerve fiber morphology and density are unaltered in *Kcna6<sup>lacZ/lacZ</sup>* mice. **A**, Representative images of epidermal innervation from the indicated hind-paw region of *Kcna6<sup>lacZ/lacZ</sup>* mice and WT littermates. In KO mice,  $\beta$ -galactosidase immunoreactivity colocalizes with the pan neuronal marker Pgp9.5 in the dermal nerve plexus. Scale bar, 15  $\mu$ m. **B**, Nerve fiber density in the epidermis did not differ significantly between KO and WT mice. Data are mean  $\pm$  SEM; mean values from individual animals.  $n = 4$  *Kcna6<sup>+/+</sup>*, 4 *Kcna6<sup>lacZ/lacZ</sup>* (2 male, 2 female per genotype).  $p = 0.4427$  (unpaired, two-tailed  $t$  test).

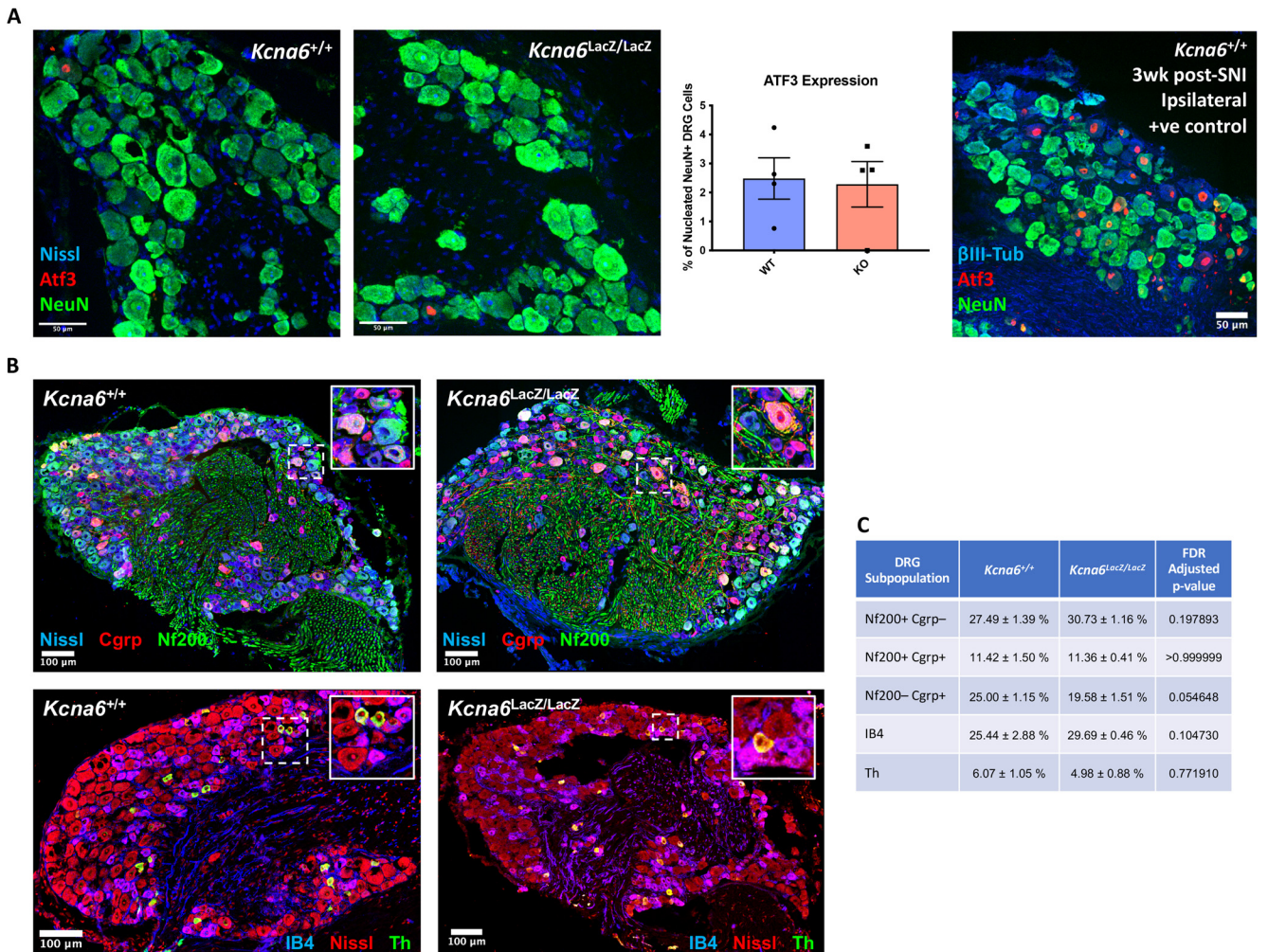


**Figure 7.** *Kcna6<sup>lacZ/lacZ</sup>* mice do not exhibit signs of cellular injury to or loss of DRG subpopulations. **A**, Despite pathology of primary afferent terminals, a lack of Atf3 upregulation suggests that injury-related gene-expression changes are not initiated in *Kcna6<sup>lacZ/lacZ</sup>* DRGs. A positive control image is provided from a WT mouse that underwent spared nerve injury. Scale bar, 50  $\mu$ m. **B**, Representative images of whole DRG sections *Kcna6<sup>lacZ/lacZ</sup>* mice and WT littermates. Inset, Magnification of dashed ROI. Sections were stained for Nf200 and Cgrp, or IB4 and Th, with a fluorescent Nissl counterstain (Neurotrace). Scale bar, 100  $\mu$ m. **C**, Mean  $\pm$  SEM percentages for each DRG subpopulation marker relative to Neurotrace (Nissl)-positive neurons. There is no significant difference between *Kcna6<sup>lacZ/lacZ</sup>* mice and WT littermates. Adjusted  $p$  values comparing genotypes are indicated from multiple unpaired  $t$  tests, performed with 5% false discovery rate using the Benjamini, Krieger, and Yekutieli two-stage setup method.  $n = 4$  *Kcna6<sup>+/+</sup>*, 4 *Kcna6<sup>lacZ/lacZ</sup>* (2 male, 2 female per genotype).

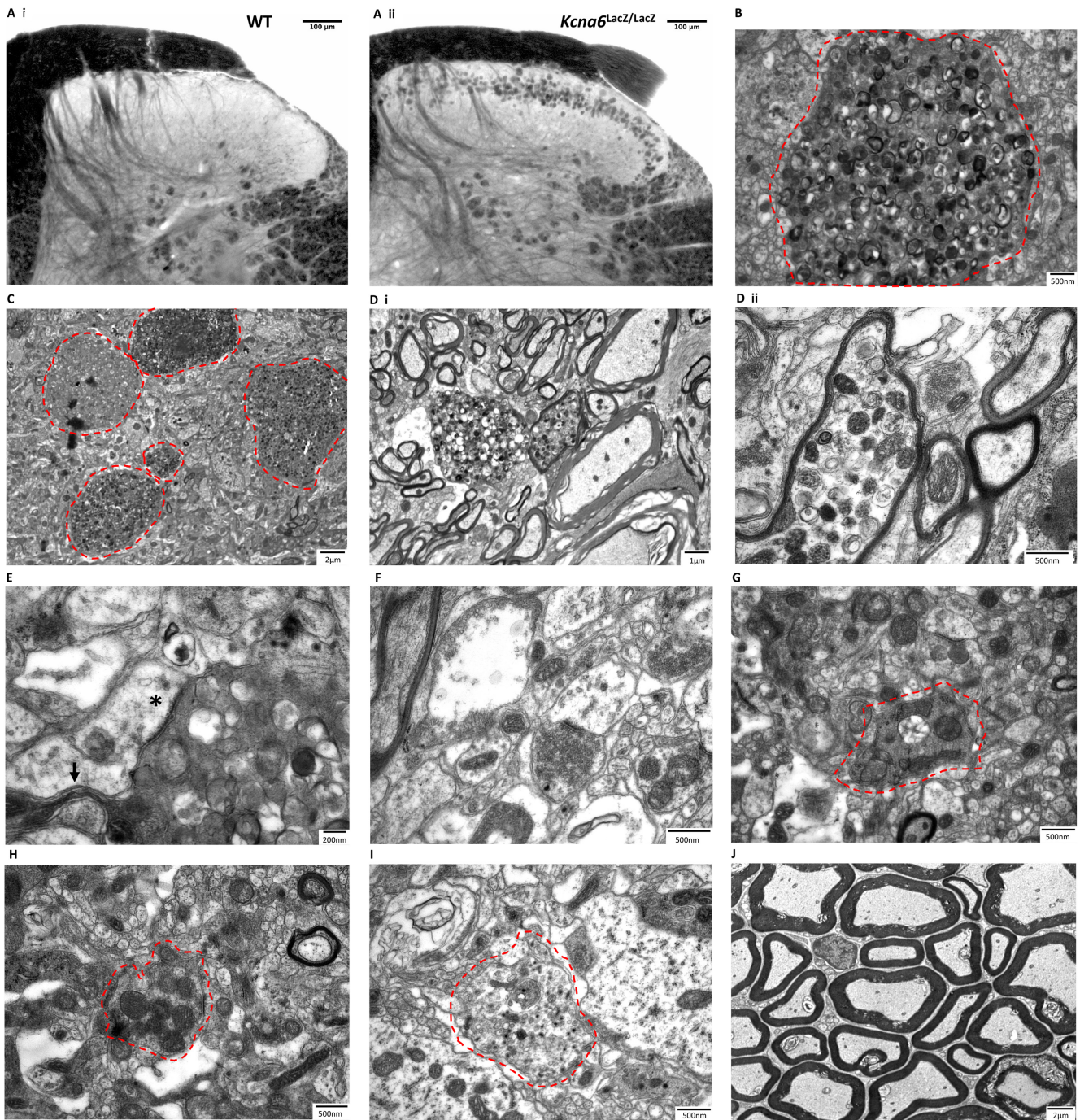


**Figure 8.** Ultrastructural analysis of degenerative *Kcna6<sup>lacZ</sup>* primary afferents. **A**, The 60- $\mu\text{m}$ -thick osmicated sections showing normal anatomy in WT tissue (**Ai**), and lipid-rich profiles in the superficial *Kcna6<sup>lacZ/lacZ</sup>* dorsal horn (**Aii**). **B**, **C**, Swollen terminals (red dashed areas) vary in size and electron density and contain many small vesicular components. **D**, Some of the abnormal vesicle-containing profiles originate from myelinated afferents in Lissauer's tract. **E**, Numerous profiles were observed adjacent to postsynaptic dendrites (asterisk) and sprouting intervaricose axons (arrow) but lacked presynaptic neurotransmitter vesicles. **F**, Some normal synapses were observed. **G**, Presumed Type I glomerular central boutons ( $C_1$ ) originating from IB4<sup>+</sup> neurons appeared abnormal, as did (**H**) presumed Type II glomerular central boutons ( $C_2$ ) and (**I**) peptidergic boutons containing dense-cored vesicles. Red dashed areas indicate the abnormal afferent terminals. **J**, Axons in the dorsal root were normal.

relate to the manipulation of the *Kcna6* locus, since WT littermates were anatomically normal and the abnormal structures in *Kcna6<sup>lacZ/lacZ</sup>* dorsal horn were intensely immunoreactive for the *lacZ* gene product  $\beta$ -galactosidase/LacZ (Fig. 4A–D). Specifically, we identified that central axonal projections of primary afferent neurons had swollen features in superficial as well as deep dorsal horn laminae. These abnormal swellings did not colocalize with neuronal (NeuN, Pax-2) or glial (Gfap, astrocytes; Iba1, microglia) markers (Fig. 4A–C). There was, however, immunohistochemical

colocalization with IB4 and Cgrp (Fig. 4D), and interbreeding *Kcna6<sup>lacZ/lacZ</sup>* mice with *Advillin-EGFP* reporter mice (MMRRC stock #034769-UCD) demonstrated colocalization of EGFP (Fig. 5A,B), confirming their primary afferent origin. The abnormal profiles were detected in both male and female *Kcna6<sup>lacZ/lacZ</sup>* mice. Some  $\beta$ -galactosidase staining distinct from the primary afferent terminals was detected throughout the gray and white matter, occasionally colocalizing with Pax-2 (Fig. 4A,B). Since this LacZ reporter is driven by the endogenous *Kcna6* promoter, this likely reflects

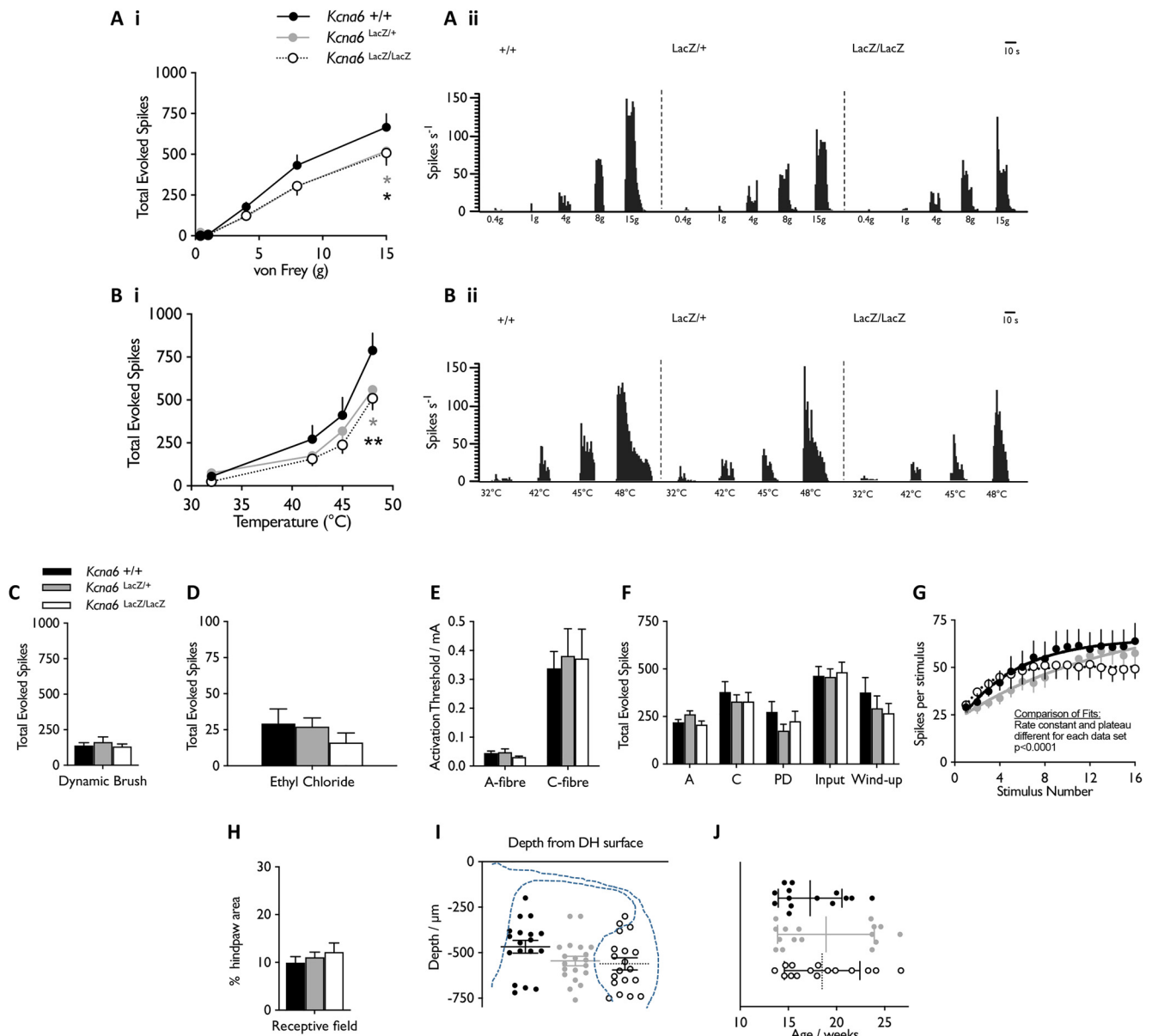


**Figure 9.** Electrophysiological characterization of *Kcna6<sup>lacZ</sup>* WDR neurons. **Ai, Bi**, Graded firing responses in WDR neurons, evoked by mechanical (von Frey) or hot water stimuli of increasing intensity applied to the hind-paw. **Aii, Bii**, Representative traces from single neurons. \**p* < 0.05, \*\**p* < 0.01 versus WT (two-way repeated-measures ANOVA with Dunnett’s *post hoc* comparison test). **C, D**, Responses evoked by dynamic application of a painter’s brush, or droplets of evaporative cooling agents. \**p* < 0.05 (ordinary one-way ANOVA, Tukey’s *post hoc* test). **E**, A- and C-fiber activation thresholds as determined by WDR response latency to electrical stimulation of the hind-paw receptive field. **F**, Total spikes attributed to A- or C-fibers, or postdischarge (PD) as determined by WDR response latency, and attributed to input versus wind-up (see Materials and Methods). **G**, Firing responses to a train of 16 identical electrical stimuli at a frequency of 0.5 Hz. **H–J**, Characterization of receptive field size (**H**), and WDR depth from the dorsal spinal cord surface (**I**), and a graphic depicting the age of mice from which WDRs were sampled. Group data are mean ± SEM in all panels except **J**, which is mean ± SD. **A–D, H, I**, *n* = 19 neurons from 14 *Kcna6<sup>+/+</sup>* (7 male, 7 female), 21 neurons from 16 *Kcna6<sup>lacZ/+</sup>* (10 male, 6 female), 19 neurons from 15 *Kcna6<sup>lacZ/lacZ</sup>* (6 male, 9 female) mice. **E–G**, *n* = 15 of these neurons per genotype had electrical properties characterized.

known low-level expression of *Kcna6* in some excitatory and inhibitory interneuron populations (Häring et al., 2018; Zeisel et al., 2018), or reported *Kcna6* expression in mouse and rat mature and progenitor oligodendrocytes (Attali et al., 1997; Chittajallu et al., 2002) and astrocytes (Smart et al., 1997; Zhu et al., 2014).

Six-week-old *Kcna6<sup>lacZ/lacZ</sup>*; *Advillin-EGFP* mice presented with clear swollen terminals, although the profiles were much reduced in size compared with at 24 weeks (Fig. 5B). Meanwhile, heterozygous *Kcna6<sup>lacZ/+</sup>* mice appeared to have a degree of protection against the development of this central terminal pathology but the phenotype progressed with increasing age (Fig. 5Ci–Ciii). No evidence of degeneration was found in WT littermates

at 11 months old (Fig. 5Civ). Compared with age-matched WT, there appeared to be no accompanying thermal hyposensitivity in a small cohort of these aged *Kcna6<sup>lacZ/+</sup>* heterozygotes (Fig. 5D), although these animals developed a structural abnormality, albeit to a lesser degree than the homozygotes. This pathology was only detected in the central terminals of *Kcna6<sup>lacZ/lacZ</sup>* primary afferents; morphology and counts of intra-epidermal nerve fiber density in the hind-paw skin were normal (Fig. 6). Pathology to sensory neuron terminals did not initiate upregulation of neural injury marker, *Atf3* (Tsujino et al., 2000), in *Kcna6<sup>lacZ/lacZ</sup>* DRG neurons relative to WT littermates and proportion of *Atf3<sup>+</sup>* DRG neurons in both genotypes was far lower

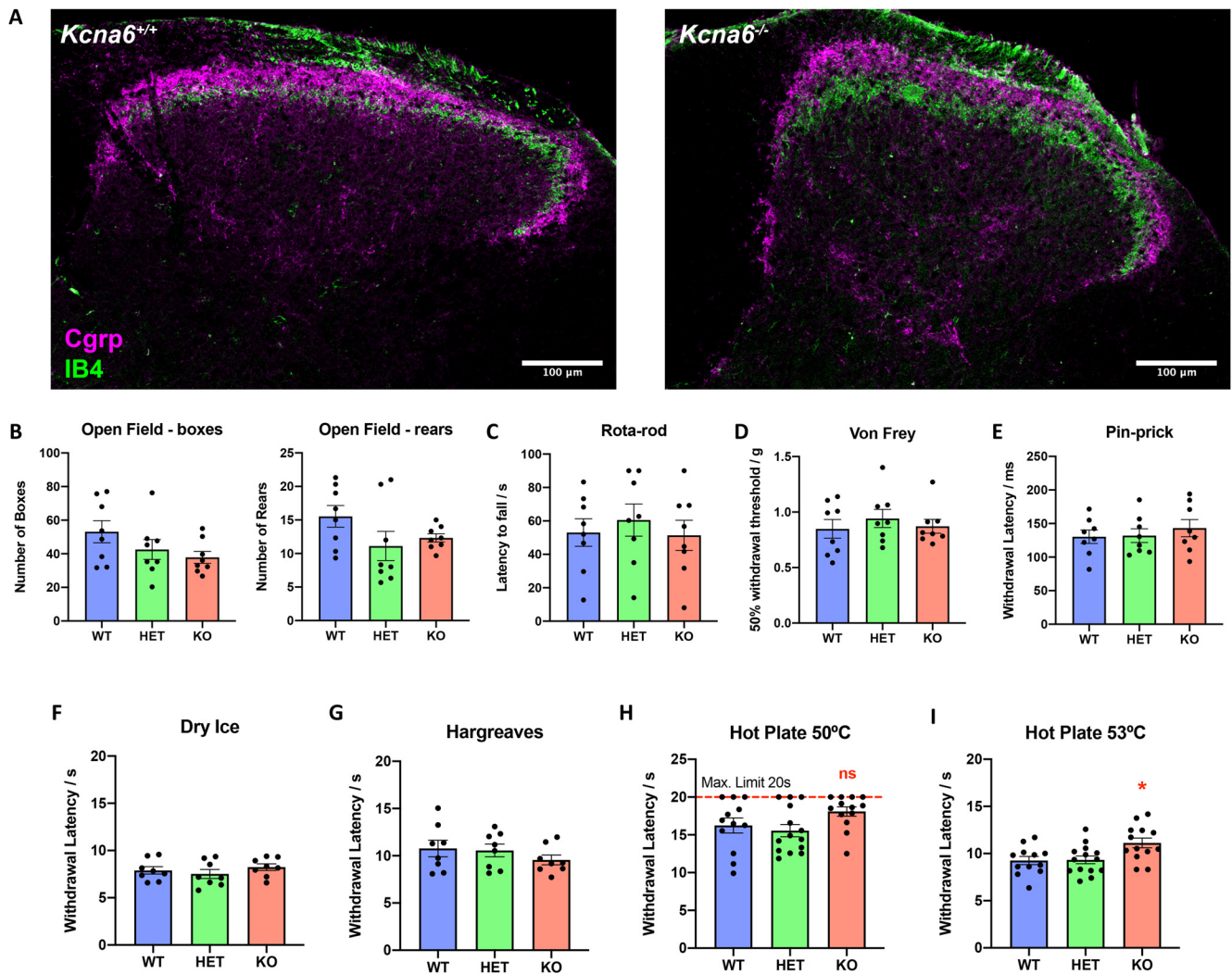


**Figure 10.** Anatomical and behavioral consequences of CRISPR-mediated *Kcna6* deletion independent of *lacZ* expression. **A**, Comparison of IB4<sup>+</sup> and Cgrp<sup>+</sup> central terminal staining in CRISPR-mediated *Kcna6*<sup>-/-</sup> homozygote KOs and WT littermates >15 weeks old reveals normal morphology. Scale bar, 100  $\mu$ m. **B**, Measurement of exploratory behavior (gridline crosses and rearing episodes) averaged across 3 baselines. **C**, Motor performance on rotarod was unaffected in *Kcna6*<sup>+/-</sup> and *Kcna6*<sup>-/-</sup> mice. **D–I**, Withdrawal threshold or latency to plantar hind-paw stimulation by von Frey (**D**), pin-prick (**E**), dry ice (**F**), Hargreaves (**G**), and hot plate (**H,I**). \**p* < 0.05 versus *Kcna6*<sup>+/-</sup> by one-way ANOVA (**I**) with Dunnett's multiple comparisons test. *n* = 8 *Kcna6*<sup>+/+</sup> (4 male, 4 female), 8 *Kcna6*<sup>+/-</sup> (4 male, 4 female), 8 *Kcna6*<sup>-/-</sup> (5 male, 3 female) (**B–G**); *n* = 12 *Kcna6*<sup>+/+</sup> (4 male, 8 female), 14 *Kcna6*<sup>+/-</sup> (6 male, 8 female), 13 *Kcna6*<sup>-/-</sup> (6 male, 7 female) (**H,I**). Data are mean  $\pm$  SEM.

than positive control DRG tissue sampled from WT mice after spared nerve injury (Decosterd and Woolf, 2000) (Fig. 7A). There was also no obvious loss of neurons in any DRG subpopulation (Fig. 7B).

TEM was used to analyze these dorsal horn structures at nanoscale. The abnormal axon terminals identified previously were stained intensely by osmium when observed using light microscopy in *Kcna6*<sup>lacZ/lacZ</sup> tissue, suggesting the presence of a high concentration of lipids (Fig. 8A*i,Aii*). TEM revealed densely packed, lipid-rich vesicular bodies contained within membrane-delimited profiles (Fig. 8B). Both the abnormal profiles and the vesicles within were highly variable in size and electron density (Fig. 8C). Some profiles were ensheathed by myelin, within or in close proximity to Lissauer's tract (Fig. 8D*i,Dii*). Others made clear synaptic contacts with adjacent dendrites containing postsynaptic densities, and often appeared to send out multiple cytoplasmic projections from their swollen region, tentatively designated as intervaricose axons (Fig. 8E).

While some normal presynaptic boutons (of unknown origin) could be found in the superficial laminae (Fig. 8F), there was a notable reduction of normal Type I (C<sub>1</sub>) and Type II (C<sub>2</sub>) glomerular

central boutons, originating from IB4<sup>+</sup> neurons and A $\delta$ - or C-LTMRs, respectively (West et al., 2015; Gutierrez-Mecinas et al., 2016; Larsson and Broman, 2019). The few examples of central glomerular boutons appeared highly irregular in form and content (Fig. 8G–I). Type I central boutons (C<sub>1</sub>) are described as having “a dark small central terminal of indented contour with closely packed spherical vesicles of variable diameter and few mitochondria” (Ribeiro-Da-Silva and Coimbra, 1982), but the example in Figure 8G lacks vesicles and is very abnormal. Some Type II central boutons (C<sub>2</sub>) and peptidergic axonal boutons (containing dense-core vesicles) were observed, although similarly these did not look normal and potentially included vesicular pathology (Fig. 8H,I). The dorsal root was unaffected (Fig. 8J), so the accumulation of membranous, vesicular bodies appeared to occur once afferents had penetrated the cord.

#### Dorsal horn WDR neurons from *Kcna6*<sup>lacZ</sup> mice have reduced electrophysiological responses to peripheral stimuli

We reasoned that the abnormality in primary afferent terminals was highly likely to underlie behavioral deficits in *Kcna6*<sup>lacZ/lacZ</sup> mice via impaired neurotransmission from first- to second-order afferent

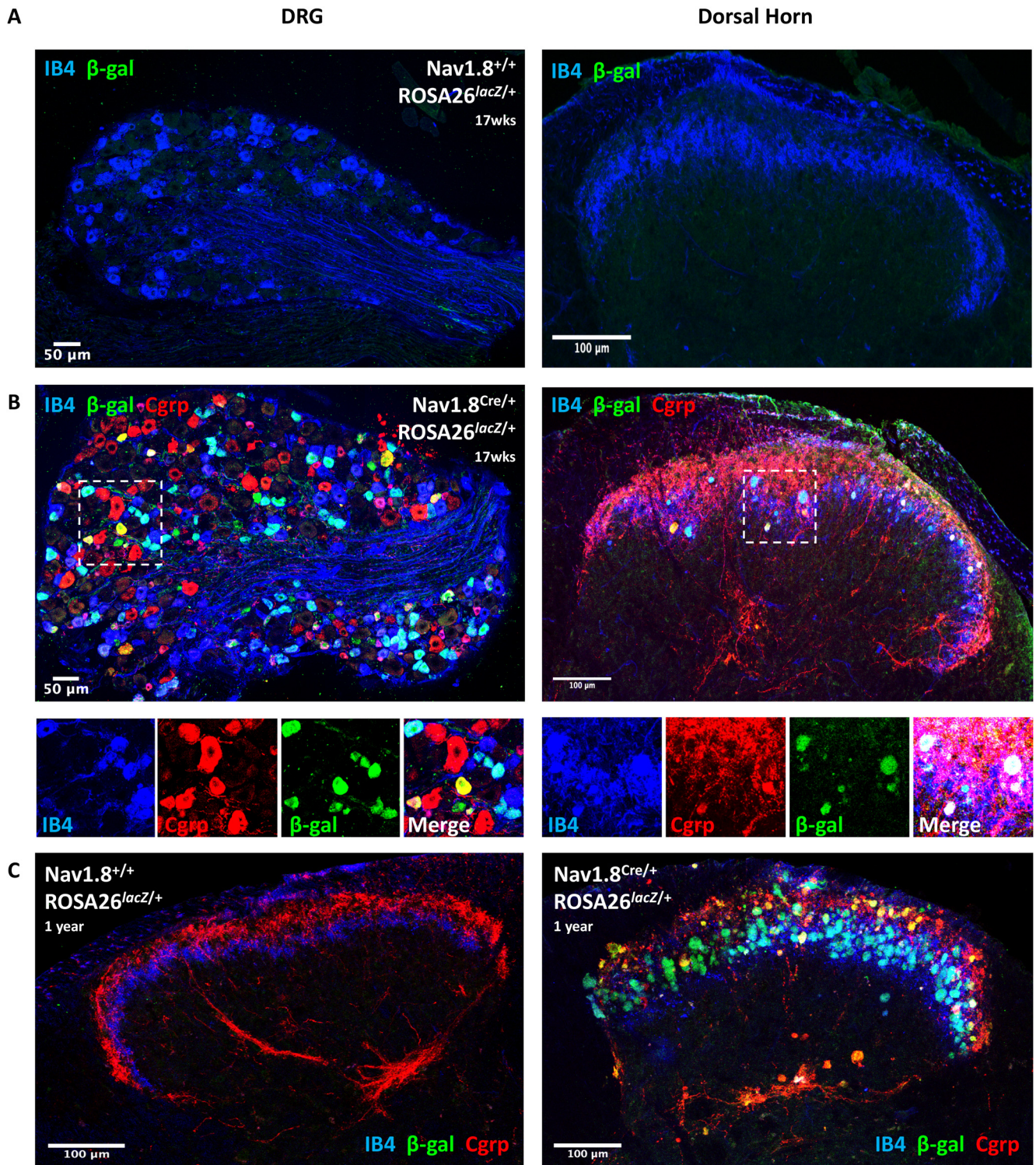


**Figure 11.** Anatomical consequences of nociceptor-specific LacZ expression independent of *Kcna6* deletion. **A**, No Cre-mediated LacZ expression in Nav1.8 Cre-negative mice >17 weeks old expressing the ROSA26<sup>lacZ</sup> reporter allele. IB4<sup>+</sup> terminals in the dorsal horn appear normal in these mice despite expressing *neo* globally. **B**, In >17-week-old mice carrying one ROSA26<sup>lacZ</sup> allele and one Nav1.8 Cre allele, *lacZ* is expressed in small-diameter, IB4<sup>+</sup> and CGRP<sup>+</sup> DRG neurons. Swollen nociceptor terminals containing  $\beta$ -galactosidase are clearly visible in the superficial laminae. **A**, **B**, Images are representative paired DRG and dorsal horn sections from the same animals. **C**, One-year-old Cre-negative mice remain phenotypically normal. In 1-year-old Nav1.8<sup>Cre/+</sup>; ROSA26<sup>lacZ/+</sup> mice, dorsal horn pathology was much more extensive, including in Cgrp<sup>+</sup> afferents projecting to deeper laminae. Scale bars: DRG, 50  $\mu$ m; dorsal horn, 100  $\mu$ m.

neurons. We therefore undertook electrophysiological analysis of the response of deep dorsal horn WDR neurons to hind-paw stimulation.

WT, *Kcna6*<sup>lacZ/+</sup>, and *Kcna6*<sup>lacZ/lacZ</sup> WDR firing rates were characterized after “natural” stimulation by calibrated von Frey

filaments, graded temperatures of water, brush, and evaporative cooling. In all genotypes, the graded intensity of mechanical and thermal stimuli was coded in the WDR firing rate, as is expected of these neurons (Fig. 9A,B). However, at the noxious end of the mechanical and thermal repertoire, there were significant deficits

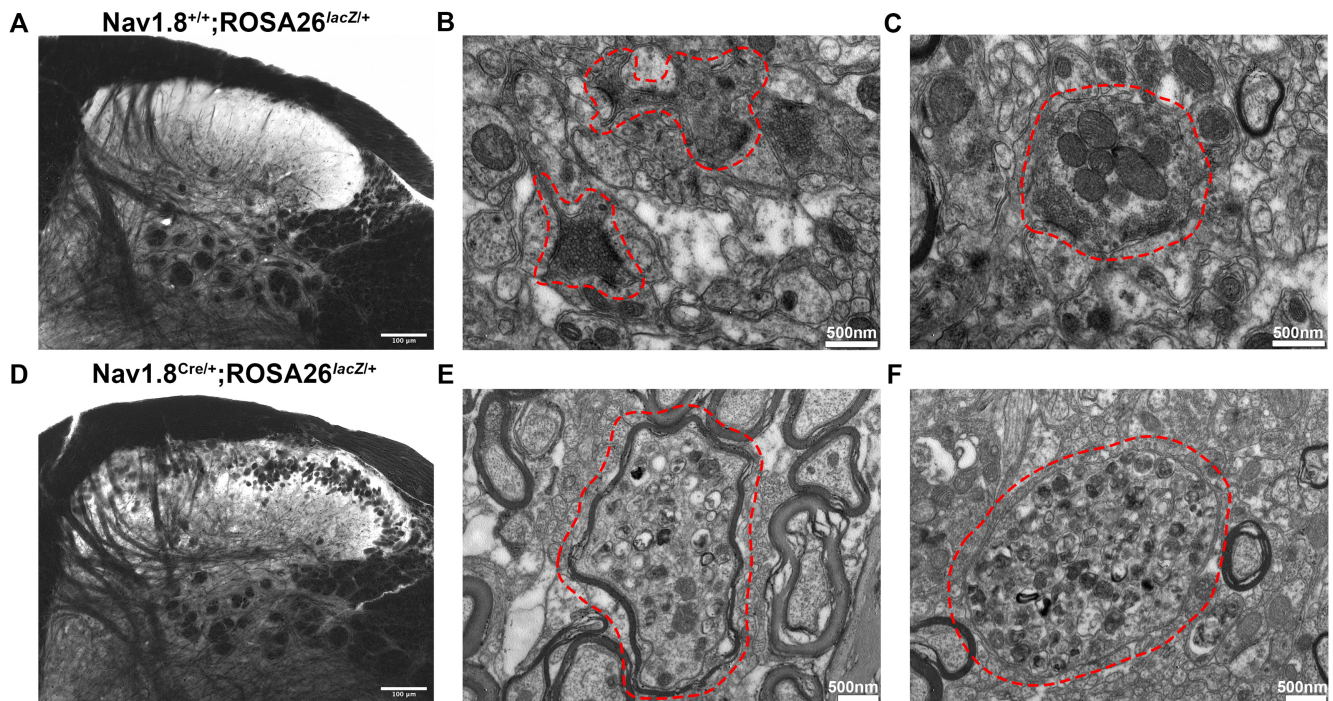


**Figure 12.** LacZ causes similar ultrastructural lipid abnormalities to nociceptor terminals when expressed in Nav1.8-Cre neurons. **A, D**, Light micrographs of osmicated dorsal horn sections from Nav1.8<sup>+/+</sup>;ROSA26<sup>lacZ/+</sup> and Nav1.8<sup>Cre/+</sup>;ROSA26<sup>lacZ/+</sup> reveals that degenerative primary afferent terminals in Nav1.8-Cre-positive mice are rich in lipid species, similarly to *Kcna6*<sup>lacZ/lacZ</sup> mice. Scale bar, 100  $\mu$ m. **B, C**, TEM imaging of Nav1.8<sup>+/+</sup>;ROSA26<sup>lacZ/+</sup> dorsal horn showing normal appearance of Type I (**B**) and Type II (**C**) glomerular central boutons (red dashed areas) forming multiple synaptic contacts in lamina II. Scale bar, 500 nm. **E, F**, TEM imaging of Nav1.8<sup>Cre/+</sup>;ROSA26<sup>lacZ/+</sup> dorsal horn sections reveals axon terminals with similar ultrastructural morphologic features to *Kcna6*<sup>lacZ/lacZ</sup> mice (red dashed areas), including numerous and varied endosomal/lysosomal-like structures within. Scale bar, 500 nm.

in spike generation in both *Kcna6*<sup>lacZ</sup> heterozygote and homozygote mice following 15 g von Frey or 48°C heat stimulation (Fig. 9A,B). Responses to non-noxious mechanical brush stimulation did not differ between genotypes (Fig. 9C). Evaporative cooling with ethyl chloride did not elicit significantly different responses across genotypes (Fig. 9D).

Electrical activation thresholds for A- and C-fiber-evoked spikes were unchanged in heterozygous or homozygous *Kcna6*<sup>lacZ</sup> animals (Fig. 9E) versus WTs, nor were there statistical differences in the total evoked spikes by either fiber class after a train of 16 electrical stimuli to the receptive field on the paw (Fig. 9F). The number of spikes generated after the C-fiber latency window (termed postdischarge) was also not affected (Fig. 9F). While the total number of spikes attributed to “wind-up” of WDRs (i.e., the progressive increase in responsiveness with each stimulus) was not different between genotypes (Fig. 9F), there were some considerable differences in the kinetics of wind-up between WTs and *Kcna6*<sup>lacZ</sup> mutants. Specifically, WDR responses in WTs followed a typical hyperbolic pattern, gradually reaching a maximal discharge rate toward the end of the 16-stimulus paradigm (Fig. 9G). KOs had a similar initial rate of wind-up but reached a lower plateau, while wind-up in heterozygotes formed a much more linear relationship with increasing stimuli. Epidermal receptive fields providing input to WDRs were similar in size across all genotypes, as was the range of sampled neuron depths and the age of mice at the time of experiment (Fig. 9H–I).

#### LacZ-negative *Kcna6*<sup>-/-</sup> mice have milder behavioral phenotypes with no pathology in presynaptic primary afferent terminals

The degenerative phenotype affecting the central terminals of primary afferents in *Kcna6*<sup>lacZ/lacZ</sup> mice was unexpected and had not previously been reported in other *Shaker*-like potassium

channel mutants. For comparison with the very unusual phenotype of the *Kcna6*<sup>lacZ</sup> strain, we characterized a different commercially available CRISPR-mediated constitutive *Kcna6* KO mouse (MMRRC stock #042391-JAX), containing no exogenous *lacZ* cassette. Spinal cord tissue was collected from these homozygous *Kcna6*<sup>-/-</sup> mice aged >15 weeks, by which time point dorsal horn pathology had fully developed in *Kcna6*<sup>lacZ/lacZ</sup> mice. However, there was no sign of a similar effect on central primary afferent terminals; the superficial dorsal horn neuropil appeared normal, with dense peptidergic and nonpeptidergic fiber reactivity in lamina II (Fig. 10A).

Responses to a wide range of sensory (noxious and non-noxious) stimuli across multiple modalities were assessed, and mice were also challenged with multiple motor tasks. Performance across tasks, such as the open field and rotarod challenges, was comparable between *Kcna6*<sup>-/-</sup>, *Kcna6*<sup>+/-</sup>, and *Kcna6*<sup>+/+</sup> littermate mice (Fig. 10B,C). Responses to punctate mechanical stimulation by von Frey hairs and more noxious pin-prick were also similar (Fig. 10D,E), as well as responses to noxious cooling of the hind-paw with the dry ice test (Fig. 10F) (Brenner et al., 2012). Compared with the phenotype of *Kcna6*<sup>lacZ</sup> KOs, the thermal hyposensitivity of this *Kcna6*<sup>-/-</sup> cohort was much milder, with no discernible difference in withdrawal latency to the Hargreaves test or a 50°C hot plate (Fig. 10G,H). However, with more intense noxious hot plate stimulation at 53°C, the *Kcna6*<sup>-/-</sup> cohort had a mildly but significantly delayed response time (Fig. 10I).

#### Nav1.8<sup>Cre/+</sup>-dependent expression of LacZ is sufficient to induce presynaptic pathology in primary afferent terminals

The absence of primary afferent degeneration in *Kcna6*<sup>-/-</sup> mice suggested that the expression of exogenous LacZ was responsible for the pathology identified in the dorsal horn of *Kcna6*<sup>lacZ</sup> mice.

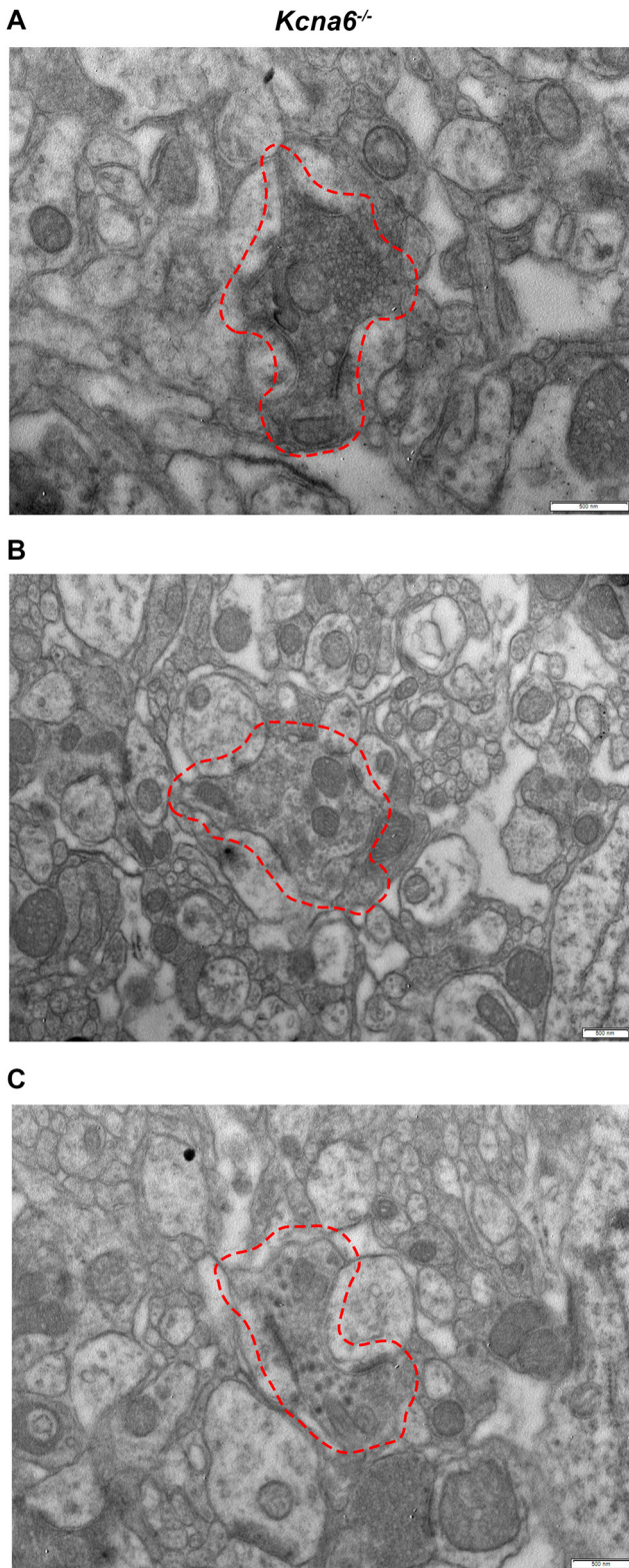


**Figure 13.** *Kcna6*<sup>-/-</sup> KO mice not expressing *lacZ* have normal morphologic dorsal horn features. **A**, Normal appearance of a Type I glomerular central bouton (red dashed area) in a *Kcna6*<sup>-/-</sup> mouse. Scale bar, 500 nm. **B**, Normal appearance of a Type II glomerular central bouton (red dashed area) in a *Kcna6*<sup>-/-</sup> mouse. Scale bar, 500 nm. **C**, Normal appearance of a peptidergic bouton (red dashed area) containing dense-core vesicles that forms two asymmetrical synapses, in a *Kcna6*<sup>-/-</sup> mouse. Scale bar, 500 nm.

However, it remained possible that this phenomenon arose because of: (1) the neomycin resistance cassette also present in the <tm1Lex> alleles of *Kcna6*<sup>lacZ</sup> mice (Fig. 3A); or (2) an unanticipated interaction between the loss of Kv1.6 subunits and expression of LacZ. To seek definitive evidence that LacZ expression alone is intrinsically harmful to the central terminals of nociceptive primary afferent neurons, we used a Nav1.8 promoter-driven Cre recombinase (Nassar et al., 2004; Stirling et al., 2005) to induce expression of exogenous LacZ (Soriano, 1999) on a *Kcna6*<sup>+/+</sup> background in primary afferent nociceptors. The breeding of Nav1.8<sup>Cre/+</sup> and ROSA26<sup>lacZ/lacZ</sup> produced Nav1.8<sup>Cre/+</sup>; ROSA26<sup>lacZ/+</sup> compound heterozygotes expressing LacZ protein in Nav1.8<sup>+</sup> neurons, which overlap considerably with *Kcna6*<sup>+</sup> neurons in the DRG (Usoskin et al., 2015; Zeisel et al., 2018; Zheng et al., 2019).

Neither LacZ protein nor dorsal horn abnormalities were detected by immunohistochemistry in 17-week-old Cre-negative Nav1.8<sup>+/+</sup>; ROSA26<sup>lacZ/+</sup> mice which, without the presence of Cre recombinase, express a neomycin resistance cassette globally (Fig. 11A). This suggests that exogenous neomycin phosphotransferase was not responsible for primary afferent terminal degeneration in *Kcna6*<sup>lacZ</sup> mice. In Nav1.8 Cre-positive mice also carrying the ROSA26<sup>lacZ</sup> allele, exogenous LacZ expression was detected and abnormal LacZ<sup>+</sup> presynaptic terminals were once again visible within the dorsal horn, colocalizing with IB4 and Cgrp staining (Fig. 11B). These were, however, less numerous than in the *Kcna6*<sup>lacZ</sup> animals at the equivalent age. Nav1.8<sup>Cre/+</sup>; ROSA26<sup>lacZ/+</sup> mice had far more extensive evidence of primary afferent degeneration in the dorsal horn at ~1 year of age, including lesions of axons within the attached dorsal root and those projecting into deeper laminae (Fig. 11C). Nav1.8 Cre-negative littermates demonstrated normal dorsal horn morphology at this time point.

Viewed with TEM, the ultrastructure of pathologic Nav1.8<sup>Cre/+</sup>; ROSA26<sup>lacZ/+</sup> afferents (Fig. 12) was similar to those of the *Kcna6*<sup>lacZ/lacZ</sup> mice (Fig. 8), while normal morphology of primary afferent terminals was observed in Nav1.8-Cre-negative littermate controls (Fig. 12) and in *Kcna6*<sup>-/-</sup> KO mice not expressing *lacZ* (Fig. 13). Clearly, the presence of exogenous LacZ protein in DRG neurons is sufficient to cause age-dependent deterioration of primary afferent presynaptic boutons.

### Ganglioside metabolism is implicated in LacZ-mediated pathophysiology

LacZ is a bacterial enzyme with  $\beta$ -galactosidase activity (Juers et al., 2012), and is therefore well placed to interfere with endolysosomal metabolism of complex gangliosides (sialic acid-containing glycosphingolipids), the major constituent of mammalian cell membranes. Neurons chiefly synthesize a- and b-series gangliosides, including GM1, cleavage of which to GM2 is achieved throughout the endo-lysosomal pathway by GM1- $\beta$ -galactosidase removing a terminal  $\beta$ -galactose residue. We hypothesized that overexpression of exogenous LacZ may result in accumulation of GM1, GM2, or other neuronal ganglioside species, and tested this using immunohistochemical techniques. GM1 is bound by cholera toxin-B (CTxB) (Merritt et al., 1994), and we identified positive staining for GM1 with fluorophore-conjugated CTxB in the dorsal root and dorsal column white matter tracts, but also colocalizing with markers of LacZ-affected nociceptor terminals from *Kcna6*<sup>lacZ/lacZ</sup> and Nav1.8<sup>Cre/+</sup>; ROSA26<sup>lacZ/+</sup> mice in the superficial dorsal horn, including Cgrp and  $\beta$ -galactosidase (Fig. 14). Other colocalizing ganglioside species were identified via monoclonal antibody staining against GD2 itself or GD3-based

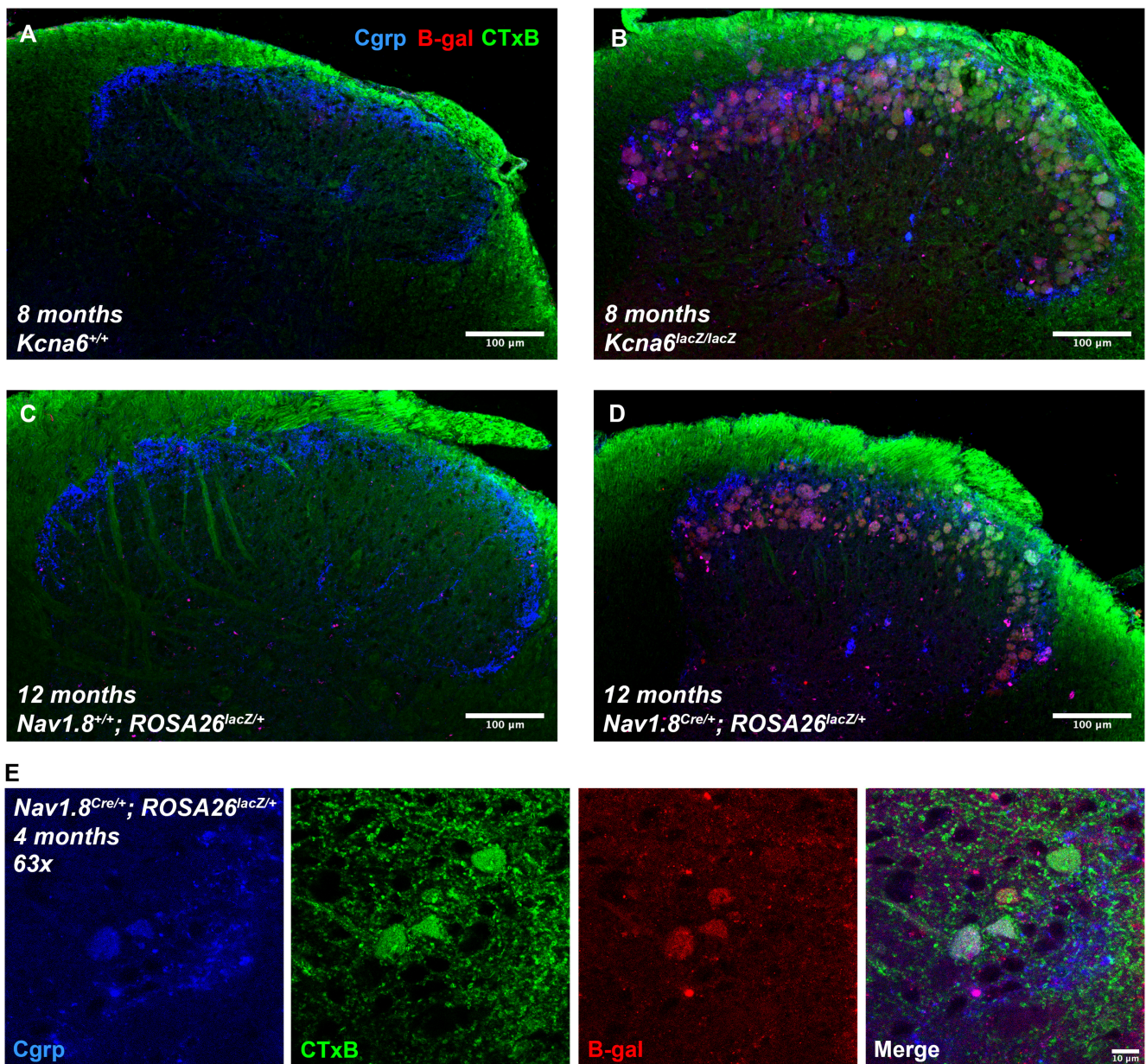


**Figure 14.** Accumulation of GM1 gangliosides in LacZ-affected primary afferent terminals. *A–D*, Staining for GM1 ganglioside with Alexa-488-conjugated CTxB reveals GM1 in primary afferent fibers in the mouse dorsal root, dorsal column white matter tracts, and dorsal horn gray matter. Additionally, in 8-month-old *Kcna6*<sup>lacZ/lacZ</sup> mice (*B*) or 12-month-old *Nav1.8*<sup>Cre/+</sup>; *ROSA26*<sup>lacZ/+</sup> mice (*D*), GM1 colocalized with aberrant afferent terminals marked by  $\beta$ -galactosidase and Cgrp immunostaining. Scale bars, 100  $\mu$ m. *E*, High-power images of *Nav1.8*<sup>Cre/+</sup>; *ROSA26*<sup>lacZ/+</sup> afferent terminals depict punctate CTxB staining in abnormal afferent terminals, colocalized with  $\beta$ -galactosidase and/or Cgrp.

derivatives GT1b/GQ1b (Boffey et al., 2005; Clark et al., 2017) (Fig. 15).

#### Mice lacking *Kcna6* exhibit prolonged mechanical and thermal hypersensitivity after peripheral nerve injury

Upregulation of *Kcna6* in painful rat and human neuromas has implicated this subunit in a compensatory response to nerve injury (Calvo et al., 2016). Furthermore, local  $\alpha$ -dendrotoxin-mediated blockade of *Kcna6*-containing channels in the context of neuroma produces a persistent mechanical hypersensitivity (Calvo et al., 2016), revealing their role in setting neuropathic mechanosensory thresholds. We investigated whether this subunit contributes to pain sensation in a similar fashion in mice, using a CCI model in *Kcna6*<sup>em1(IMPC)</sup> mice lacking *Kcna6* but not expressing *lacZ*. At baseline, as per Figure 10, *Kcna6* KOs

were again hyposensitive to 53°C but not 50°C noxious heat in a TPP assay versus 25°C (Fig. 16*A,B*), and displayed no difference in sensitivity to Hargreaves or von Frey assays compared with littermate controls retaining a functional *Kcna6* allele (Fig. 16*A,B*). Behavioral outcomes were followed for 28 d after injury. Across 50°C TPP, Hargreaves, and von Frey assays, both cohorts developed thermal and mechanical hypersensitivity by 7 d after injury (Fig. 16*A,C,D*). With follow-up across all of these assays, mice completely lacking *Kcna6* remained persistently hypersensitive compared with littermate controls, which displayed a degree of recovery from the initial day 7 hypersensitivity (Fig. 16*A,C,D*). Only homozygous *Kcna6*-null mice exhibited an observable injury-mediated hypersensitivity on 53°C versus 25°C TPP because of their baseline hyposensitivity; however, in the post-injury period, there were discernible differences between *Kcna6*<sup>-/-</sup>



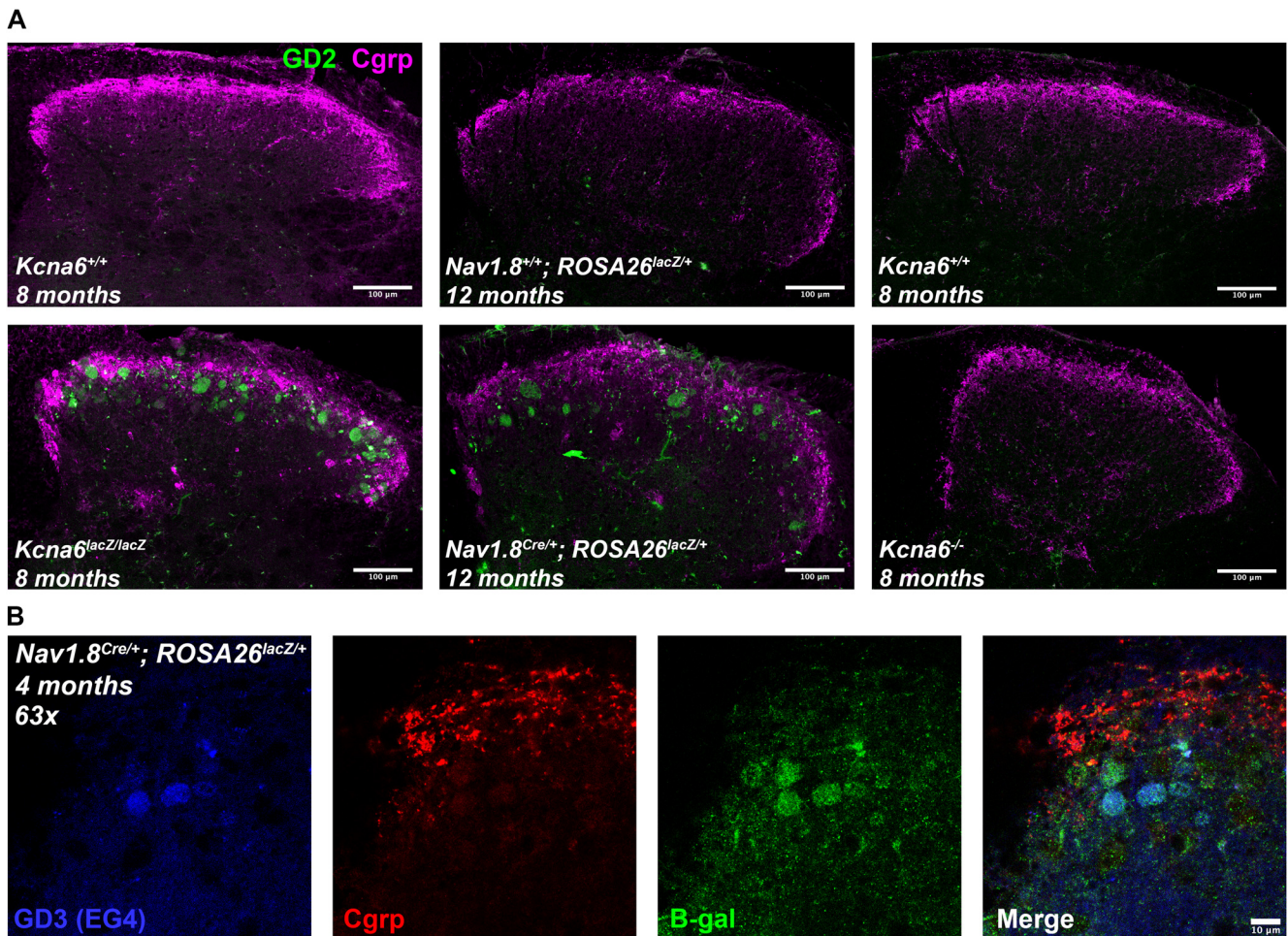


**Figure 15.** Multiple ganglioside species accumulate in LacZ-affected primary afferent terminals. **A**, Mouse monoclonal antibodies raised against ganglioside GD2 label degenerating nociceptor terminals in *Kcna6*<sup>lacZ/lacZ</sup> and *Nav1.8*<sup>Cre/+</sup>; *ROSA26*<sup>lacZ/+</sup> mice, but not (non-LacZ) *Kcna6*<sup>-/-</sup> mice or littermate controls of any strain. Scale bars, 100  $\mu$ m. **B**, Mouse anti-GD3 (EG4) antibodies also label GT1b/GQ1b, colocalizing with some  $\beta$ -galactosidase-positive terminals in lamina II of the superficial dorsal horn. Scale bar, 10  $\mu$ m.

and *Kcna6*<sup>+/-</sup> mice at day 28 whereby *Kcna6*-null mice were hypersensitive compared with littermate controls (Fig. 16B).

## Discussion

### Neurotoxicity of exogenous LacZ expression

Through investigation of several transgenic mouse strains, a major finding was that exogenous *lacZ* cassettes expressed in primary afferent nociceptors cause pathologic accumulation of lipid species within central presynaptic arborizations. These lipid-rich “organelles” resemble endo-/lyso-/autophagosomal structures involved in turnover of plasma membrane gangliosides (Figs. 8 and 12). Loss-of-function mutations affecting GM1- $\beta$ -galactosidase or the group of enzymes that catabolize GM2 ( $\beta$ -hexosaminidases) result in fatal neurodegenerative ganglioside storage disorders (Breiden and Sandhoff, 2019), with accumulation of the substrates GM1 and GM2, respectively, in neuronal lysosomes.

GM1 and GM2 gangliosidoses feature “ballooned” axons (Breiden and Sandhoff, 2019), visible by Golgi staining in feline models (Purpura and Baker, 1978; Walkley et al., 1981) but also present in postmortem brain tissue from human patients (Sandhoff and Harzer, 2013). Ultrastructurally, these “meganeurites” contain electron-dense membranous whorls and lysosome-like structures (Purpura and Baker, 1978; Purpura et al., 1978;

Walkley et al., 1981, 1990; Sango et al., 1995) remarkably similar to swollen terminals of *Kcna6*<sup>lacZ/lacZ</sup> and *Nav1.8*<sup>Cre/+</sup>; *ROSA26*<sup>lacZ/+</sup> afferents (Figs. 8C–J and 12E,F). Similar vacuolated “inclusion bodies” were identified via TEM in DRG neurons from  $\alpha$ -galactosidase KO mice in a Fabry disease model (Miller et al., 2018).

Endogenous  $\beta$ -galactosidase is undetectable in WT primary afferents by immunohistochemistry (Fig. 2), or RNA sequencing (Zeisel et al., 2018). We argue that exogenous LacZ/ $\beta$ -galactosidase overrides endogenous ganglioside metabolism, resulting in aberrant accumulation of several ganglioside species identified via immunostaining (Figs. 14 and 15). Within the DRG, GM1 gangliosides are mostly associated with large myelinated primary afferent neurons (Robertson and Grant, 1989), and GM1 staining is almost absent from the superficial dorsal horn in mice, although GM1 upstream precursors GD1a, GD1b, and GT1b are abundant (Vajn et al., 2013). We clearly labeled GM1-, GD2-, and GD3-derived gangliosides in LacZ-affected terminals, suggesting that endogenous ganglioside metabolism was being diverted through abnormal biochemical pathways (Breiden and Sandhoff, 2019).

Endogenous GM1- $\beta$ -galactosidase expression accumulates over time and is a marker of cellular senescence (Dimri et al., 1995; Lee et al., 2006; Geng et al., 2010). GM2 gangliosidoses, including Tay-Sachs disease and Sandhoff disease, have an early

onset, although variants with delayed onset and reduced severity correlate with improved catabolic GM2 clearance (Leinekugel et al., 1992; Sandhoff and Harzer, 2013; Breiden and Sandhoff, 2019). LacZ-induced ganglioside accumulation may therefore accelerate cellular aging processes, consistent with slower pathologic progression in *Kcna6<sup>lacZ/+</sup>* heterozygotes (Fig. 5) and *Nav1.8<sup>Cre/+</sup>;ROSA26<sup>lacZ/+</sup>* mice (Fig. 11B,C), which only expressed one *lacZ* allele. Another feature of GM2 gangliosidosis, demyelination, involves microglia (Ogawa et al., 2018), which were also detected adjacent to swollen *Kcna6<sup>lacZ</sup>* profiles (Fig. 4C).

Although LacZ was detectable in *Kcna6<sup>lacZ/lacZ</sup>* distal nerve terminals innervating glabrous skin (Fig. 6), structural abnormalities were only observed in central afferent axons, mostly once they had penetrated the spinal cord but occasionally in the dorsal root of severely affected, aged animals. This is curious and accentuates the polarized structure and function of sensory neurons. It remains unclear why presynaptic axons were affected specifically, but neurotransmitter release is dependent on effective lysosomal and ganglioside function (Hirai et al., 2005), impaired in acquired autoimmune diseases, such as Guillain-Barré syndrome (Buchwald et al., 2007; Plomp and Willison, 2009). Gangliosides, such as GM1, can colocalize with presynaptic proteins in lipid rafts (Taverna et al., 2004), known to regulate exocytosis (Salaün et al., 2004). Age-related presynaptic accumulation of GM1 also initiates degenerative change via amyloid deposition (Yamamoto et al., 2008).

We noted a predominant effect on nociceptive versus non-nociceptive afferent terminals in *Kcna6<sup>lacZ/lacZ</sup>* mice, which likely reflects the higher expression of Kv1.6 (and hence LacZ) in nociceptors (Figs. 1 and 2). Peptidergic and nonpeptidergic nociceptors form morphologically distinct specialized central boutons (Ribeiro-Da-Silva and Coimbra, 1982; West et al., 2015; Gutierrez-Mecinas et al., 2016; Larsson and Broman, 2019). The propensity for degeneration of IB4<sup>+</sup> more than Cgrp<sup>+</sup> terminals is interesting; it suggests that these subpopulations may express distinct species of gangliosides or rely on differential ganglioside metabolism to maintain presynaptic bouton integrity. IB4-binding terminals retract following peripheral nerve injury (Tajti et al., 1988; Molander et al., 1996; Shehab et al., 2004), whereas both IB4<sup>+</sup> and Cgrp<sup>+</sup> terminals retract following systemic administration of HIV therapeutic stavudine (Huang et al., 2013). These findings might probe further investigation into the role of ganglioside metabolism in maintaining primary afferent synaptic structures, especially in the context of peripheral neuropathy.

Our focus has been on *lacZ* expression in DRG neurons; one previous study has investigated expression in cortical neurons and raised concerns regarding the use of LacZ reporters (Reichel et al., 2016). The authors found that *lacZ* expression in cortical glutamatergic neurons caused severe morphologic and

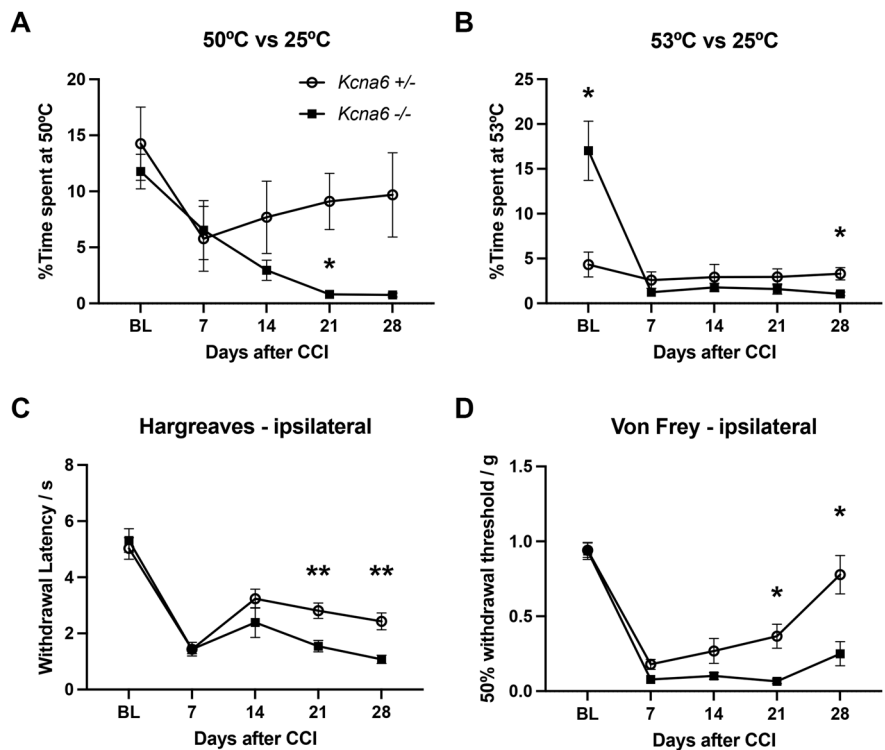


**Figure 16.** Mice lacking *Kcna6* suffer persistent mechanical and thermal hypersensitivity after CCI of the sciatic nerve. **A**, **B**, Time spent at 50°C versus 25°C (**A**) or 53°C versus 25°C (**B**) was recorded over 2 min to assess TPP before and after peripheral nerve injury in *Kcna6<sup>+/-</sup>* and *Kcna6<sup>-/-</sup>* mice. **C**, The Hargreaves assay was used to assess thermal sensitivity thresholds in the hind-paw ipsilateral to nerve injury. **D**, Stimulation of the ipsilateral hind-paw by von Frey hairs was used to assess mechanical sensitivity thresholds. \* $p < 0.05$ , \*\* $p < 0.01$ , *Kcna6<sup>-/-</sup>* versus *Kcna6<sup>+/-</sup>* by two-way repeated-measures ANOVA with Geisser-Greenhouse correction for sphericity and Sidak *post hoc* multiple comparison test.  $n = 10$  *Kcna6<sup>+/-</sup>*, 9 *Kcna6<sup>-/-</sup>* (age- and sex-matched). Data are mean  $\pm$  SEM.

behavioral impairments, such as decreased hippocampal volume, reduced dendritic branching in hippocampal neurons, and deficits in hippocampus-dependent memory. They did not report abnormal lipid accumulations in axon terminals, although it is possible that these were not specifically sought. Our combined findings from *lacZ* expression in central and peripheral neurons mean that anatomic, electrophysiological, and behavioral data from transgenic mice expressing *lacZ* require interpretation with extreme caution. We advocate using alternative reporters, such as GFP or YFP, and note we and others have not observed any abnormalities in primary afferent terminals of *Advillin*-EGFP mice (Sikandar et al., 2017; Hunter et al., 2018). This is particularly relevant as a significant proportion of the lines produced in high throughput phenotypic screens, such as the International Mouse Phenotyping Consortium, use LacZ as a reporter (Skarnes et al., 2011; Meehan et al., 2017).

### The role of Kv1.6 in thermosensation

This study also revealed a role for Kv1.6 in regulating thermal sensitivity. The unexpected neurodegenerative phenotype of LacZ-expressing animals was considered likely to underlie the differences in severity of thermal behavioral phenotypes between *Kcna6<sup>lacZ/lacZ</sup>* and *Kcna6<sup>-/-</sup>* mice, especially since Gb3 ganglioside accumulation in Fabry disease models was shown to interfere with Trpv1 signaling and heat sensation (Hofmann et al., 2018). The intricate mechanisms through which gangliosides modulate pain sensation specifically, including regulation of ion channels and receptors, have been reviewed recently

**Table 1. Appendix**

Antigen	Host/conjugate	Source/RRID	Dilution	
<b>Antibodies</b>				
<i>Primary antibodies</i>				
Atf3	Rabbit	Santa Cruz Biotechnology (sc188) RRID:AB_2258513	1:500	
$\beta$ -III tubulin	Mouse	Sigma-Aldrich (T8578) RRID:AB_1841228	1:500	
$\beta$ -gal ( <i>E. coli</i> )	Chicken	Abcam (ab9361) RRID:AB_307210	1:500	
Cgrp	Sheep	Enzo Life Sciences (BML-CA1137) RRID:AB_2050885	1:500	
Cgrp	Rabbit	Peninsula Laboratories (T-4032) RRID:AB_2313775	1:500	
IB4	(biotinylated)	Sigma-Aldrich (LT-2140) RRID:AB_2313663	1:200	
GD2	Mouse	Kindly gifted by Dr. Juliet Gray, University of Southampton	2 $\mu$ g/ml	
GD3 (EG4)	Mouse	As per Boffey et al. (2005) and Clark et al. (2017)	2 $\mu$ g/ml	
Gfap	Mouse	Sigma-Aldrich	1:500	
Glutamine synthetase	Rabbit	Sigma-Aldrich (G2781) RRID:AB_259853	1:1000	
Homer1	Goat	Frontier Institute RRID:AB_2631104	1:500	
Iba1	Rabbit	Abcam (ab178847)	1:500	
NeuN	Chicken	Millipore (ABN91) RRID:AB_11212808	1:500	
NeuN	Rabbit	Abcam (ab177487) RRID:AB_2532109	1:500	
Neurotrace (red)	NA	Invitrogen (N21482) RRID:AB_2620170	1:100	
Neurotrace (blue)	NA	Invitrogen (N21479)	1:100	
NF200	Mouse	Sigma-Aldrich (N-0142) RRID:AB_477257	1:500	
Pax2	Rabbit	Thermo Fisher Scientific (71-6000) RRID:AB_2533990	1:200	
Pgp9.5	Rabbit	Ultradone (discontinued)	1:500	
Synaptophysin	Rabbit	Frontier Institute RRID:AB_2571842	1:500	
Th	Sheep	Millipore (AB1542) RRID:AB_90755	1:200	
<i>Secondary antibodies</i>				
Biotin	Streptavidin/Pacific Blue	Thermo Fisher Scientific (S11222)	1:500	
Chicken IgG	Goat/Alexa-488	Thermo Fisher Scientific (A-11039)	1:500	AB_2534096
Chicken IgG	Goat/Alexa546	Thermo Fisher Scientific (A-11040)	1:500	AB_2534097
GM1	Cholera toxin B/Alexa-488	Invitrogen (C34775)	2 $\mu$ g/ml	NA
Goat IgG	(biotinylated)	Vector Laboratories (BA-9500)	1:200	AB_2336123
Mouse IgG	Goat/Pacific Blue	Thermo Fisher Scientific (P-31582)	1:500	AB_10374586
Mouse IgG	Donkey/Alexa-488	Thermo Fisher Scientific (A-21202)	1:500	AB_141607
Rabbit IgG	Donkey/Cy3	Jackson ImmunoResearch Laboratories (711-166-152)	1:500	AB_2313568
Rabbit IgG	Donkey/Alexa-488	Thermo Fisher Scientific (A-21206)	1:500	AB_2535792
Rabbit IgG	Goat/Pacific Blue	Thermo Fisher Scientific (P-10994)	1:500	AB_2539814
Sheep IgG	Donkey/Alexa-488	Thermo Fisher Scientific (A-11015)	1:500	AB_2534082
Gene	Description	Forward (5'-3')	Reverse (5'-3')	
<b>qRT-PCR primers</b>				
<i>Kcna6</i> #1	Coding sequence	TGGCGAGGATGAGAAACCAC	TACTGAGACGATGGCGATGC	
<i>Kcna6</i> #2	Coding sequence	CCAGCTTCGACGCTATCCTT	TGGTTTCATCCTCGCCAC	
<i>Kcna1</i>	Exon-spanning	TTACCTGGGCACGGAGATA	ACACCCTACCAAGCGGATG	
<i>Kcna2</i>	Exon-spanning	CATCTGCAAGGGCAACGTAC	CCTTTGGAAGGAAGGAGGCA	
<i>Hprt1</i>	Exon-spanning	GTCTGTGGCCATCTGCTAG	TGGGGACGCAGCACTGACA	
<i>Gapdh</i>	Exon-spanning	TGTGTCCGCTGTGGATCTGA	TTGCTGTGAAGTCGCAGGAG	

(Sántha et al., 2020). The common feature between the two strains was hyposensitivity to noxious heat. At present, it is unclear through what mechanism this hyposensitivity manifests.

Most known functions of Kv1 channels would instead predict a hypersensitive phenotype on removal of Kv1.6. Its upregulation following peripheral nerve injury in WT animals reduces spontaneous electrical discharge in injured nerve fibers and behavioral hypersensitivity, while pharmacological blockade of Kv1.6 in this context maintains spontaneous discharge and persistent mechanical hypersensitivity (Calvo et al., 2016). Blockade of Kv1 currents in nonpeptidergic nociceptors isolated from Mrgprd-GFP mice (where Kv1.6 is the major Kv1 subunit) also increased their maximal action potential firing rate substantially (Zheng et al., 2019). The channel's acute effect on membrane excitability thus limits excitability, in line with canonical Kv1 channel properties in neurons (Browne et al., 1994; Smart et al., 1998; Glazebrook et al., 2002; Chi and Nicol, 2007; Robbins and Tempel, 2012; Hao et al., 2013; Dawes et al., 2018). We had therefore been expecting, if anything, thermal hypersensitivity.

It is possible that these paradoxical effects relate to subunit stoichiometry of heteromeric Kv1 channels, which can significantly influence activation thresholds. Kv1.2 subunits promote a more depolarized activation potential than Kv1.1 (Akhtar et al., 2002), and Kv1.6 a still more depolarized activation potential (Grupe et al., 1990) ( $V_{0.5max}$  for homomeric channels: Kv1.1,  $-33$  mV; Kv1.2,  $-26$  mV; Kv1.6,  $-17$  mV). KO of Kv1.6 in sensory neurons could result in overrepresentation of Kv1.1/1.2 subunits and reduced neuronal excitability. It is noted that *Kcna6* is expressed throughout the mouse nervous system (Zeisel et al., 2018); and in two global Kv1.6 KO strategies, there are myriad explanations for hyposensitive behavioral traits, requiring further interrogation.

### *Kcna6* promotes recovery from nerve injury

Intriguingly, in the context of neuropathic CCI, *Kcna6*-null animals behave in a more canonical fashion, displaying more severe and prolonged hypersensitivity to thermal and mechanical stimuli, while littermate controls with functioning Kv1.6 gradually recover. We were able to observe the hyposensitive phenotype to acute noxious thermal stimuli reported in both *Kcna6* KO strains (Figs. 3 and 10) and the persistent post-neuropathic hypersensitive phenotypes predicted by Calvo et al. (2016), in the same cohort of animals (Fig. 16). We believe this reconciles the two contrasting datasets and provides robust evidence that both phenomena are genuine consequences of Kv1.6 loss of function.

In conclusion, we have identified a role for Kv1.6 subunits in acute thermal nociception and the recovery response to nerve injury. We also present evidence that transgenic insertion of exogenous *lacZ*-containing cassettes can have pathologic downstream consequences for neuronal structure and function. LacZ induced accumulation of gangliosides in presynaptic primary nociceptor terminals in the dorsal horn. This anatomic defect exacerbated the underlying behavioral phenotype of Kv1.6 KO mice, demonstrated by comparison between *Kcna6<sup>lacZ</sup>* and CRISPR-mediated *Kcna6<sup>-/-</sup>* mice. This confirms that exogenous *lacZ* cassettes can be markedly neurotoxic. We recommend caution when interpreting past and future results from transgenic mice expressing exogenous LacZ. We also illustrate a role for Kv1.6 in the recovery of normal sensory function following nerve injury, thus enhancing that Kv1.6 function could be a therapeutic target in neuropathic pain.

## References

- Akhtar S, Shamotienko O, Papakosta M, Ali F, Dolly JO (2002) Characteristics of brain Kv1 channels tailored to mimic native counterparts by tandem linkage of  $\alpha$  subunits: implications for  $K^+$  channelopathies. *J Biol Chem* 277:16376–16382.
- Attali B, Wang N, Kolot A, Sobko A, Cherepanov V, Soliven B (1997) Characterization of delayed rectifier Kv channels in oligodendrocytes and progenitor cells. *J Neurosci* 17:8234–8245.
- Bennett GJ, Xie YK (1988) A peripheral mononeuropathy in rat that produces disorders of pain sensation like those seen in man. *Pain* 33:87–107.
- Boffey J, Odaka M, Nicoll D, Wagner ER, Townson K, Bowes T, Conner J, Furukawa K, Willison HJ (2005) Characterisation of the immunoglobulin variable region gene usage encoding the murine anti ganglioside antibody repertoire. *J Neuroimmunol* 165:92–103.
- Breiden B, Sandhoff K (2019) Lysosomal glycosphingolipid storage diseases. *Annu Rev Biochem* 88:461–485.
- Brenner DS, Golden JP, Gereau IR (2012) A novel behavioral assay for measuring cold sensation in mice. *PLoS One* 7:e39765.
- Browne DL, Ganchar ST, Nutt JG, Brunt ER, Smith EA, Kramer P, Litt M (1994) Episodic ataxia/myokymia syndrome is associated with point mutations in the human potassium channel gene, KCNA1. *Nat Genet* 8:136–140.
- Buchwald B, Zhang G, Vogt-Eisele AK, Zhang W, Ahangari R, Griffin JW, Hatt H, Toyka KV, Sheikh KA (2007) Anti ganglioside antibodies alter presynaptic release and calcium influx. *Neurobiol Dis* 28:113–121.
- Calvo M, Richards N, Schmid AB, Barroso A, Zhu L, Ivulic D, Zhu N, Anwandter P, Bhat MA, Court FA, McMahon SB, Bennett DL (2016) Altered potassium channel distribution and composition in myelinated axons suppresses hyperexcitability following injury. *Elife* 5:e12661.
- Chi XX, Nicol GD (2007) Manipulation of the potassium channel Kv1.1 and its effect on neuronal excitability in rat sensory neurons. *J Neurophysiol* 98:2683–2692.
- Chittajallu R, Chen Y, Wang H, Yuan X, Ghiani CA, Heckman T, McBain CJ, Gallo V (2002) Regulation of Kv1 subunit expression in oligodendrocyte progenitor cells and their role in G<sub>1</sub>/S phase progression of the cell cycle. *Proc Natl Acad Sci USA* 99:2350–2355.
- Clark AJ, Kaller MS, Galino J, Willison HJ, Rinaldi S, Bennett DL (2017) Co-cultures with stem cell-derived human sensory neurons reveal regulators of peripheral myelination. *Brain* 140:898–913.
- Dawes JM, Weir GA, Middleton SJ, Patel R, Chisholm KI, Pettingill P, Peck LJ, Sheridan J, Shakir A, Jacobson L, Gutierrez-Mecinas M, Galino J, Walcher J, Kühnemund J, Kuehn H, Sanna MD, Lang B, Clark AJ, Themistocleous AC, Iwagaki N, et al. (2018) Immune or genetic-mediated disruption of CASPR2 causes pain hypersensitivity due to enhanced primary afferent excitability. *Neuron* 97:806–822.
- Decosterd I, Woolf CJ (2000) Spared nerve injury: an animal model of persistent peripheral neuropathic pain. *Pain* 87:149–158.
- Dimri GP, Lee X, Basile G, Acosta M, Scott G, Roskelley C, Medrano EE, Linskens M, Rubelj I, Pereira-Smith O, Peacocke M, Campisi J (1995) A biomarker that identifies senescent human cells in culture and in aging skin in vivo. *Proc Natl Acad Sci USA* 92:9363–9367.
- Dixon WJ (1965) The up-and-down method for small samples. *J Am Stat Assoc* 60:967–978.
- Geng YQ, Guan JT, Xu XH, Fu YC (2010) Senescence-associated beta-galactosidase activity expression in aging hippocampal neurons. *Biochem Biophys Res Commun* 396:866–869.
- Glazebrook PA, Ramirez AN, Schild JH, Shieh CC, Doan T, Wible BA, Kunze DL (2002) Potassium channels Kv1.1, Kv1.2 and Kv1.6 influence excitability of rat visceral sensory neurons. *J Physiol* 541:467–482.
- González A, Ugarte G, Restrepo C, Herrera G, Piña R, Gómez-Sánchez JA, Pertusa M, Orio P, Madrid R (2017) Role of the excitability brake potassium current I<sub>KD</sub> in cold allodynia induced by chronic peripheral nerve injury. *J Neurosci* 37:3109–3126.
- Grupe A, Schroter KH, Ruppertsberg JP, Stocker M, Drewes T, Beckh S, Pongs O (1990) Cloning and expression of a human voltage-gated potassium channel: a novel member of the RCK potassium channel family. *EMBO J* 9:1749–1756.
- Gutierrez-Mecinas M, Kuehn ED, Abaira VE, Polgár E, Watanabe M, Todd AJ (2016) Immunostaining for Homer reveals the majority of excitatory synapses in laminae I–III of the mouse spinal dorsal horn. *Neuroscience* 329:171–181.

- Hao J, Padilla F, Dandonneau M, Lavebratt C, Lesage F, Noël J, Delmas P (2013) Kv1.1 channels act as mechanical brake in the senses of touch and pain. *Neuron* 77:899–914.
- Häring M, Zeisel A, Hochgerner H, Rinwa P, Jakobsson JE, Lönnerberg P, La Manno G, Sharma N, Borgius L, Kiehn O, Lagerström MC, Linnarsson S, Ernfors P (2018) Neuronal atlas of the dorsal horn defines its architecture and links sensory input to transcriptional cell types. *Nat Neurosci* 21:869–880.
- Hirai H, Pang Z, Bao D, Miyazaki T, Li L, Miura E, Parris J, Rong Y, Watanabe M, Yuzaki M, Morgan JI (2005) Cbln1 is essential for synaptic integrity and plasticity in the cerebellum. *Nat Neurosci* 8:1534–1541.
- Hofmann L, Hose D, Griefshammer A, Blum R, Döring F, Dib-Hajj S, Waxman S, Sommer C, Wischmeyer E, Üçeyler N (2018) Characterization of small fiber pathology in a mouse model of Fabry disease. *Elife* 7:e39300.
- Hong DH, Li H, Kim HW, Kim HS, Son YK, Yang SR, Park JR, Ha KS, Han ET, Hong SH, Firth AL, Na SH, Park WS (2016) Alterations of voltage-dependent K<sup>+</sup> channels in the mesenteric artery during the early and chronic phases of diabetes. *Clin Exp Pharmacol Physiol* 43:808–817.
- Huang W, Calvo M, Karu K, Olausen HR, Bathgate G, Okuse K, Bennett DL, Rice ASC (2013) A clinically relevant rodent model of the HIV antiretroviral drug stavudine induced painful peripheral neuropathy. *Pain* 154:560–575.
- Hunter DV, Smaila BD, Lopes DM, Takatoh J, Denk F, Ramer MS (2018) Advillin is expressed in all adult neural crest-derived neurons. *eNeuro* 5:ENEURO.0077-18.2018.
- Ishikawa K, Tanaka M, Black JA, Waxman SG (1999) Changes in expression of voltage-gated potassium channels in dorsal root ganglion neurons following axotomy. *Muscle Nerve* 22:502–507.
- Juergens DH, Matthews BW, Huber RE (2012) LacZ  $\beta$ -galactosidase: structure and function of an enzyme of historical and molecular biological importance. *Protein Sci* 21:1792–1807.
- Larsson M, Broman J (2019) Synaptic organization of VGLUT3 expressing low-threshold mechanosensitive C fiber terminals in the rodent spinal cord. *eNeuro* 6:ENEURO.0007-19.2019.
- Lee BY, Han JA, Im JS, Morrone A, Johung K, Goodwin EC, Kleijer WJ, DiMaio D, Hwang ES (2006) Senescence-associated  $\beta$ -galactosidase is lysosomal  $\beta$ -galactosidase. *Aging Cell* 5:187–195.
- Leinekugel P, Michel S, Conzelmann E, Sandhoff K (1992) Quantitative correlation between the residual activity of  $\beta$ -hexosaminidase A and arylsulfatase A and the severity of the resulting lysosomal storage disease. *Hum Genet* 88:513–523.
- Leith JL, Koutsikou S, Lumb BM, Apps R (2010) Spinal processing of noxious and innocuous cold information: differential modulation by the periaqueductal gray. *J Neurosci* 30:4933–4942.
- Livak KJ, Schmittgen TD (2001) Analysis of relative gene expression data using real-time quantitative PCR and the 2- $\Delta\Delta$ CT method. *Methods* 25:402–408.
- Madrid R, De La Peña E, Donovan-Rodriguez T, Belmonte C, Viana F (2009) Variable threshold of trigeminal cold-thermosensitive neurons is determined by a balance between TRPM8 and Kv1 potassium channels. *J Neurosci* 29:3120–3131.
- Meehan TF, Conte N, West DB, Jacobsen JO, Mason J, Warren J, Chen CK, Tudose I, Relac M, Matthews P, Karp N, Santos L, Fiegel T, Ring N, Westerberg H, Greenaway S, Sneddon D, Morgan H, Codner GF, Stewart ME, et al. (2017) Disease model discovery from 3,328 gene knockouts by the International Mouse Phenotyping Consortium. *Nat Genet* 49:1231–1238.
- Merritt EA, Sixma TK, Kalk KH, van Zanten BA, Hol WG (1994) Galactose-binding site in *Escherichia coli* heat-labile enterotoxin (LT) and cholera toxin (CT). *Mol Microbiol* 13:745–753.
- Miller JJ, Aoki K, Moehring F, Murphy CA, O'Hara CL, Tiemeyer M, Stucky CL, Dahms NM (2018) Neuropathic pain in a Fabry disease rat model. *JCI Insight* 3:e99171.
- Molander C, Wang HF, Rivero-Melián C, Grant G (1996) Early decline and late restoration of spinal cord binding and transganglionic transport of isolectin B4 from *Griffonia simplicifolia* I after peripheral nerve transection or crush. *Restor Neurol Neurosci* 10:123–133.
- Nassar MA, Stirling LC, Forlani G, Baker MD, Matthews EA, Dickenson AH, Wood JN (2004) Nociceptor-specific gene deletion reveals a major role for Nav1.7 (PN1) in acute and inflammatory pain. *Proc Natl Acad Sci USA* 101:12706–12711.
- Ogawa Y, Irisa M, Sano T, Yanagi Y, Furusawa E, Saito T, Yamanaka S, Itoh K, Sakuraba H, Oishi K (2018) Improvement in dysmyelination by the inhibition of microglial activation in a mouse model of Sandhoff disease. *Neuroreport* 29:962–967.
- Plomp JJ, Willison HJ (2009) Pathophysiological actions of neuropathy-related anti ganglioside antibodies at the neuromuscular junction. *J Physiol* 587:3979–3999.
- Purpura DP, Baker HJ (1978) Meganeurites and other aberrant processes of neurons in feline GM1 gangliosidosis: a Golgi study. *Brain Res* 143:13–26.
- Purpura DP, Pappas GD, Baker HJ (1978) Fine structure of meganeurites and secondary growth processes in feline GM1 gangliosidosis. *Brain Res* 143:1–12.
- Reichel JM, Bedenk BT, Gassen NC, Hafner K, Bura SA, Almeida-Correa S, Genewsky A, Dedic N, Giesert F, Agarwal A, Nave KA, Rein T, Czisch M, Deussing JM, Wotjak CT (2016) Beware of your Cre-Action: lacZ expression impairs neuronal integrity and hippocampus-dependent memory. *Hippocampus* 26:1250–1264.
- Ribeiro-Da-Silva A, Coimbra A (1982) Two types of synaptic glomeruli and their distribution in laminae I-III of the rat spinal cord. *J Comp Neurol* 209:176–186.
- Robbins CA, Tempel BL (2012) Kv1.1 and Kv1.2: similar channels, different seizure models. *Epilepsia* 53 Suppl 1:134–141.
- Robertson B, Grant G (1989) Immunocytochemical evidence for the localization of the GM1 ganglioside in carbonic anhydrase-containing and RT 97-immunoreactive rat primary sensory neurons. *J Neurocytol* 18:77–86.
- Salaün C, James DJ, Chamberlain LH (2004) Lipid rafts and the regulation of exocytosis. *Traffic* 5:255–264.
- Sandhoff K, Harzer K (2013) Gangliosides and gangliosidoses: principles of molecular and metabolic pathogenesis. *J Neurosci* 33:10195–10208.
- Sango K, Yamanaka S, Hoffmann A, Okuda Y, Grinberg A, Westphal H, McDonald MP, Crawley JN, Sandhoff K, Suzuki K, Proia RL (1995) Mouse models of Tay-Sachs and Sandhoff diseases differ in neurologic phenotype and ganglioside metabolism. *Nat Genet* 11:170–176.
- Sántha P, Dobos I, Kis G, Jancsó G (2020) Role of gangliosides in peripheral pain mechanisms. *Int J Mol Sci* 21:1005.
- Shehab SA, Spike RC, Todd AJ (2004) Do central terminals of intact myelinated primary afferents sprout into the superficial dorsal horn of rat spinal cord after injury to a neighboring peripheral nerve? *J Comp Neurol* 474:427–437.
- Sikandar S, West SJ, McMahon SB, Bennett DL, Dickenson AH (2017) Sensory processing of deep tissue nociception in the rat spinal cord and thalamic ventrobasal complex. *Physiol Rep* 5:e13323.
- Skarnes WC, Rosen B, West AP, Koutourakis M, Bushell W, Iyer V, Mujica AO, Thomas M, Harrow J, Cox T, Jackson D, Severin J, Biggs P, Fu J, Nefedov M, De Jong PJ, Stewart AF, Bradley A (2011) A conditional knockout resource for the genome-wide study of mouse gene function. *Nature* 474:337–344.
- Smart SL, Bosma MM, Tempel BL (1997) Identification of the delayed rectifier potassium channel, Kv1.6, in cultured astrocytes. *Glia* 20:127–134.
- Smart SL, Lopantsev V, Zhang CL, Robbins CA, Wang H, Chiu SY, Schwartzkroin PA, Messing A, Tempel BL (1998) Deletion of the K(v)1.1 potassium channel causes epilepsy in mice. *Neuron* 20:809–819.
- Soriano P (1999) Generalized lacZ expression with the ROSA26 Cre reporter strain. *Nat Genet* 21:70–71.
- Stirling LC, Forlani G, Baker MD, Wood JN, Matthews EA, Dickenson AH, Nassar MA (2005) Nociceptor-specific gene deletion using heterozygous Nav1.8-Cre recombinase mice. *Pain* 113:27–36.
- Tajti J, Fischer J, Knyihár-Csillik E, Csillik B (1988) Transganglionic regulation and fine structural localization of lectin-reactive carbohydrate epitopes in primary sensory neurons of the rat. *Histochemistry* 88:213–218.
- Taverna E, Saba E, Rowe J, Francolini M, Clementi F, Rosa P (2004) Role of lipid microdomains in P/Q-type calcium channel (Cav2.1) clustering and function in presynaptic membranes. *J Biol Chem* 279:5127–5134.
- Tsujino H, Kondo E, Fukuoka T, Dai Y, Tokunaga A, Miki K, Yonenobu K, Ochi T, Noguchi K (2000) Activating transcription factor 3 (ATF3) induction by axotomy in sensory and motoneurons: a novel neuronal marker of nerve injury. *Mol Cell Neurosci* 15:170–182.
- Uosokin D, Furlan A, Islam S, Abdo H, Lönnerberg P, Lou D, Hjerling-Leffler J, Haeggström J, Kharchenko O, Kharchenko PV, Linnarsson S, Ernfors P (2015) Unbiased classification of sensory neuron types by large-scale single-cell RNA sequencing. *Nat Neurosci* 18:145–153.

- Vajn K, Viljetić B, Degmečić IV, Schnaar RL, Heffer M (2013) Differential distribution of major brain gangliosides in the adult mouse central nervous system. *PLoS One* 8:e75720.
- Walkley SU, Wurzelmann S, Purpura DP (1981) Ultrastructure of neurites and meganeurites of cortical pyramidal neurons in feline gangliosidosis as revealed by the combined Golgi-EM technique. *Brain Res* 211:393–398.
- Walkley SU, Baker HJ, Rattazzi MC (1990) Initiation and growth of ectopic neurites and meganeurites during postnatal cortical development in ganglioside storage disease. *Brain Res Dev Brain Res* 51:167–178.
- Watson C, Paxinos G, Kayalioglu G, Heise C (2009) Atlas of the rat spinal cord. In: *The spinal cord*, pp 238–306. San Diego: Academic.
- West SJ, Bannister K, Dickenson AH, Bennett DL (2015) Circuitry and plasticity of the dorsal horn: toward a better understanding of neuropathic pain. *Neuroscience* 300:254–275.
- Yamamoto N, Matsubara T, Sato T, Yanagisawa K (2008) Age-dependent high-density clustering of GM1 ganglioside at presynaptic neuritic terminals promotes amyloid  $\beta$ -protein fibrillogenesis. *Biochim Biophys Acta* 1778:2717–2726.
- Zeisel A, Hochgerner H, Lönnerberg P, Johnsson A, Memic F, van der Zwan J, Häring M, Braun E, Borm LE, La Manno G, Codeluppi S, Furlan A, Lee K, Skene N, Harris KD, Hjerling-Leffler J, Arenas E, Ernfors P, Marklund U, Linnarsson S (2018) Molecular architecture of the mouse nervous system. *Cell* 174:999–1014.e22.
- Zhao X, Tang Z, Zhang H, Atianjoh FE, Zhao JY, Liang L, Wang W, Guan X, Kao SC, Tiwari V, Gao YJ, Hoffman PN, Cui H, Li M, Dong X, Tao YX (2013) A long noncoding RNA contributes to neuropathic pain by silencing *Kcna2* in primary afferent neurons. *Nat Neurosci* 16:1024–1031.
- Zheng Y, Liu P, Bai L, Trimmer JS, Bean BP, Ginty DD (2019) Deep sequencing of somatosensory neurons reveals molecular determinants of intrinsic physiological properties. *Neuron* 103:598–616.e7.
- Zhu J, Yan J, Thornhill WB (2014) The Kv1.3 potassium channel is localized to the cis-Golgi and Kv1.6 is localized to the endoplasmic reticulum in rat astrocytes. *FEBS J* 281:3433–3445.